Astronomy & Astrophysics manuscript no. output
June 29, 2026

Large or bright satellite constellations

Effects on observations, including background sky brightness

O. R. Hainaut[1, 2, ⋆]

[1] European Southern Observatory, Karl-Schwarzschild-Straße 2, 85748 Garching-bei-München, Germany
[2] IAU Centre for the Protection of the Dark and Quiet Sky, IAU-UAI Headquarters, 98-bis Blvd Arago, 75014, Paris, France

-

ABSTRACT

Context. Large satellite constellations impact astronomy through both visible trails and the generation of diffuse and atmospherically scattered light. Quantification of this cumulative sky-background component is essential to assess the full ramifications of extant and proposed systems.
Aims. This study evaluates the effect of proposed constellations — ranging from current deployments to mega-constellations and very bright reflector concepts — on direct trail losses, diffuse background, and scattered sky brightness.
Methods. The methodology employs a numerical model for Mie and Rayleigh scattering in the V band, adapted from moonlight sky-brightness calculations and validated against observations of moonlight and stellar background light. This is combined with the SatConAnalytic package to quantify scattered light, diffuse light from undetected satellites, and direct losses from detected trails.
Results. Constellations comprising $\sim$ 60 000 satellites that adhere to the $V_{550\ \mathrm{km}} \geq 7$ recommendation exert a negligible effect on sky brightness, contributing only about 10^{-4} of the natural dark sky. Conversely, mega-constellations with 10^6 satellites render trails pervasive, thereby affecting the majority of long exposures. Bright satellites, such as spacecraft analogous to AST SpaceMobile, significantly impact saturating detectors even when their number is moderate. Extremely bright satellites pose a far more severe threat: a 5000-satellite Reflect Orbital-like constellation could elevate the scattered sky background by 20%–30%, and a population of 50 000 could increase it by 200%–300%.
Conclusions. The constellations currently proposed for launch, which exceed 1 700 000 objects and include satellites brighter than $V_{550\ \mathrm{km}} = 7$, would substantially degrade astronomical observations. Maintaining satellite brightness below $V_{550\ \mathrm{km}} = 7$ is important for all instruments but critical for safeguarding saturating instruments, such as the Rubin LSST camera, and for limiting sky-background pollution. Even under this constraint, the total satellite population should remain below $\sim$ 100 000 satellites to ensure that field-of-view losses do not exceed typical technical downtime.

Key words. light pollution – atmospheric effects – site testing – space vehicles – telescopes – surveys

1. Introduction

The darkness of the sky background is one of the key parameters determining the quality of an observatory: for any background-dominated observation, the exposure time required to reach a given signal-to-noise ratio (S/N) scales linearly with sky brightness. This is also critical for γ- and cosmic-ray observations based on Cherenkov radiation from cascades of secondary particles produced when the primary particle interacts with atoms in the atmosphere, for which a stable, dark background is essential.

Because of this linear dependence of exposure time on sky brightness, critical observations in the visible can be carried out only from sites with the darkest possible skies, during moonless nights. Moonlight precludes such observations, and telescopes typically switch instead to infrared instruments, for which moonlight is not an issue. Light pollution from cities and industries can raise sky brightness by orders of magnitude over distances of up to hundreds of kilometres (Cinzano et al. 2001). Professional observatories have therefore retreated to remote sites in search of the darkest skies. The best sites have a level of light pollution below 1% of the natural dark-sky brightness. Light pollution at the 10% level is incompatible with state-of-the-art observatories Walker et al. (2020). The effects of artificial light at night (ALAN) and possible mitigation methods are well documented (for a review, see Barentine 2025).

New satellite constellations are being announced, some extremely large and others extremely bright. In this work, we evaluated their contribution to scattered and diffuse light in the optical regime and discuss their direct effects on observations.

Since the spectacular launch of the first batch of SpaceX's Starlink satellites in May 2019, the number of artificial satellites orbiting the Earth has increased from ~2000 to over 14 000, dominated by the deployment of the Starlink telecommunication constellation and a few other smaller constellations. That number rises further to over 32 000 when including dead satellites and debris (from Jonathan McDowell's satellite statistics web page[1], Feb. 2026).

The early spectacular satellite 'photo-bombing' of wide-field images[2] triggered a reaction from the astronomical community. This resulted in a series of publications investigating the number and visibility period of the constellation satellites (e.g. McDowell 2020), as well as quantifying their impact on astronomical observations (e.g. Hainaut & Williams 2020;

⋆ Corresponding author: ohainaut@eso.org

[1] Jonathan McDowell's satellite statistics page
[2] e.g. this example from DECam: `https://noirlab.edu/public/images/iotw1946a/`

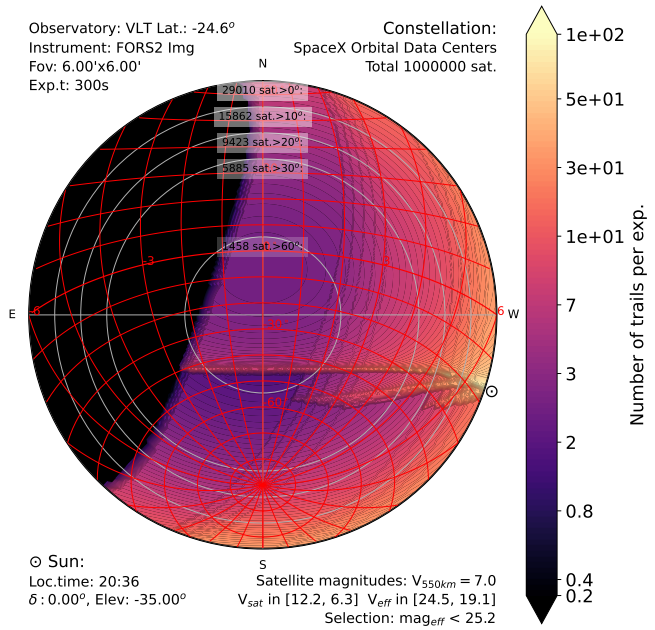

Fig. 1. Example of the effect of SpaceX's one-million-satellite Orbital Data Center constellation on a 300-second FORS2 exposure at Paranal. Even 1.3 h after the end of astronomical twilight, more than half the sky remains affected, with an average of more than eight satellite trails per image at zenith. In regions corresponding to the constellation cusps, more than 20 trails cross each image. The effect on a 15-second exposure with the 3° LSST camera at the Rubin observatory is similar. This figure shows a map of the sky above the observatory (top left), with the zenith at the centre and the horizon along the outer circle. The dark region towards the east corresponds to the part of the sky where the satellites are already in the Earth's shadow and are therefore invisible. The ⊙ symbol on the horizon indicates the Sun's azimuth; its position is given at the bottom left. The sky maps in this paper correspond to solar elevations $e_\odot \leq -21°$, i.e. well after astronomical twilight. The red grid marks hour angle and declination. The grey circles correspond to elevations of 10°, 20°, 30°, and 60° above the horizon (most observations are made above 30°). The colour scale on the right gives, in this example, the number of satellite trails per exposure. The annotations at the top right and bottom right give details of the satellite constellation and the characteristics of the individual satellites.

Bassa et al. 2022). In parallel, international conferences were organized – SatCon-1 (Walker et al. 2020) and -2 (Hall et al. 2021), Dark and Quiet Skies 1 (D&QS, Walker et al. 2020) and -2 (Walker et al. 2021) – where the optical and radio astronomy communities met with the satellite industry and relevant policy-makers. One of the key recommendations resulting from the SatCon conferences is that satellites must be fainter than magnitude $V = 7$ and, for satellites with altitudes higher than 550 km, fainter than $7+2.5\log_{10}(h/550\,\mathrm{km})$, where h is the satellite altitude in kilometres. This recommendation from the original SatCon-1 conference was endorsed by the IAU (Boley et al. 2025; IAU-CPS et al. 2024). The purely geometrical dependence with altitude would imply a factor of 5 instead of 2.5 in the expression, but the latter accounts for the fact that the decrease in apparent brightness with altitude is offset by the decrease in apparent angular velocity. This ensures that the satellites are not visible to the naked eye (with $V = 7$ corresponding to the approximate limiting magnitude of a perfect, fully dark-adapted eye under optimal observing conditions) and that they do not saturate the detector of the NSF-DOE Vera C. Rubin Observatory (see Sect. 2.1 for more details on this).

Large satellite constellations also have a significant impact on radio astronomy. This is obvious if a satellite's directional antenna directly illuminates a radio telescope pointing at that satellite. There is also a cumulative impact through the side lobes of the satellites and the telescopes, as well as through unintended emissions by the satellites. The SatCon and D&QS reports also discuss these matters. In what follows, we focus on the optical regime.

Since the first launches, a series of mitigation methods have been implemented to reduce satellite brightness. Some are operational (such as adjusting the satellite attitude or the solar panel angle), some are at the design level (e.g. covering the nadir-pointing face of the satellite with a specular coating that reflects sunlight away from Earth). SpaceX makes their findings available (SpaceX 2022). Mitigation techniques are also being developed to minimize the number of satellite trails in observations (Bassa et al. 2022) and to detect trails (Stoppa et al. 2024; Chen et al. 2025) so they can be masked (Hasan et al. 2022).

The numerous launches required putting a large number of satellites into orbit. Their operation and the eventual return of these satellites burning in the upper atmosphere also raise a series of concerns beyond the interference with optical and radio astronomy. These include the sustainability of a low-Earth orbit populated by many thousands of satellites, the associated generation of space debris, atmospheric pollution caused by the launches and re-entries, to name a few. (see Lawrence et al. 2022, for a summary).

Kocifaj et al. (2021) investigated the effect of an increased number of space debris associated with a large satellite population on the diffuse sky background. Using the available debris size distribution and scaling their number to the satellite population, they concluded that these debris could contribute 16.2 μcd m^{-2} (24.6 magnitude per square arcsecond or MpSA), and could even reach 21.1 μcd m^{-2} (24.3 MpSA) at the end of astronomical twilight, i.e. about 10% of the luminance of the dark sky (the magnitude and illuminance, surface brightness and luminance units; their conversions are discussed below and detailed in Appendix B). While this study should be refined, it shows that space debris have the potential to increase sky brightness to a level that would interfere with astronomical observations.

Bassa et al. (2022) assessed the impact of ∼60 000 satellites with a zenith apparent magnitude scaled to an altitude of 550 km $V_{550\ \mathrm{km}} = 7$. They concluded that, in the optical domain, mitigation was possible but required efforts at all stages: satellites and constellation design and operation, observation scheduling and execution, and data processing.

Since then, a series of developments has taken place:

- The number of foreseen satellites has dramatically increased. McDowell currently lists 1 766 623 planned satellites[3], dominated by SpaceX's Orbital Data Centers (one million satellites), E-Space's Cinnamon (over three-hundred-thousand satellites), and China's CTC-1 and -2 constellations (close to one-hundred-thousand satellites each), over a total of 33 large constellations.
- Satellite operators are now launching very large satellites, whose size is dominated by a large antenna enabling direct broadband communication with standard smartphones. For instance, AST SpaceMobile launched their 'BlueWalker' prototypes with a 64 m^2 antenna and $V = 0$–4 mag ($V =$

[3] Jonathan McDowell's constellation list, as of Feb. 2026

1.4 on average, Mallama et al. 2022), and they are now deploying their 'BlueBird' satellites with a 223 m^2 antenna. Mallama & Cole (2025) report their brightness around $V_{550\,\mathrm{km}} = 3.12$, i.e. $\sim$ 36× brighter than the recommended limit. Their apparent magnitudes (Cole et al. 2025) are in the 0–7 range, i.e. up to 660× brighter than the recommended limit. Other operators are also considering launching large satellites. For instance, SpaceX's 'V3', of which they plan to manufacture 5 000 per year, are described as being 'the size of roughly a 737 [Boeing plane][4]'. No magnitude measurement is available yet, but they could easily breach the $V > 7$ IAU recommendation.

– A new type of constellation aims at providing reflected sunlight to specific locations during the night, either for direct illumination or to extend the working hours of solar power stations. For that purpose, Reflect Orbital plans[5] to launch over 5000 satellites by 2030, providing light for 2 h per night, then over 50 000 satellites by 2035, providing '24/7' illumination. They indicate that large mirror-like satellites could illuminate a region across 5 km. The exact specifications of the satellites are not yet available, but it is suggested the satellites could be 54×54 m or $\sim$ 3000 m^2. While Reflect Orbital indicates that they will avoid directly illuminating observatories with the specular reflected sunlight beam, it is expected that the surface of the reflector will not be perfect and that part of the light will be diffused.

The direct effect of these satellites can be estimated using existing methods, such as the Bassa et al. (2022) analytical model. As an example, Fig. 1 illustrates that, even well into the astronomical night, each and every observation will be affected by numerous satellite trails over most of the sky. Even if the satellites are fainter than $V_{550\,\mathrm{km}}$, all will result in well-detected trails. These direct effects are discussed below.

A completely different impact, not considered until now, is the effect of light scattered by the atmosphere. In the optical domain, the main component of dark sky luminance is the airglow, i.e. the emission by upper-atmosphere molecules, followed by the zodiacal light, i.e. sunlight scattered by interplanetary dust, the integrated starlight, and the extragalactic background light. In their reference paper on the night sky, Leinert et al. (1998) detail these different sources in the optical domain, from ultraviolet to infrared. The relative contribution of these components varies by orders of magnitude. The airglow varies with atmospheric conditions; Barentine (2022) provide a detailed discussion of these contributions and their variations. The zodiacal light depends on the ecliptic latitude and the difference in longitude with the Sun. The stellar background changes with galactic latitude and longitude. Masana et al. (2021) show the seasonal variations of these components in their Fig. 11. Patat (2003) reports their variations as measured from Paranal, Chile. Based on these results, contributions to an optimal dark sky (i.e. measured away from the Milky Way and zodiacal light and excluding individual contributions from stars) are about 60% for airglow, 30% for zodiacal light, 4% for scattered starlight. The remainder corresponds to galactic and extragalactic diffuse light. Based on Leinert et al. (1998) and Patat (2003), we used $V = 22$ MpSA as the reference for the surface brightness of a pure, dark sky at zenith. This surface brightness is equivalent to a luminance of 174μcd m^{-2} ; see Appendix B for details and Bará et al. (2020) for a discussion. Any additional light source illuminating the atmosphere – natural or artificial – contributes to the scattered light background.

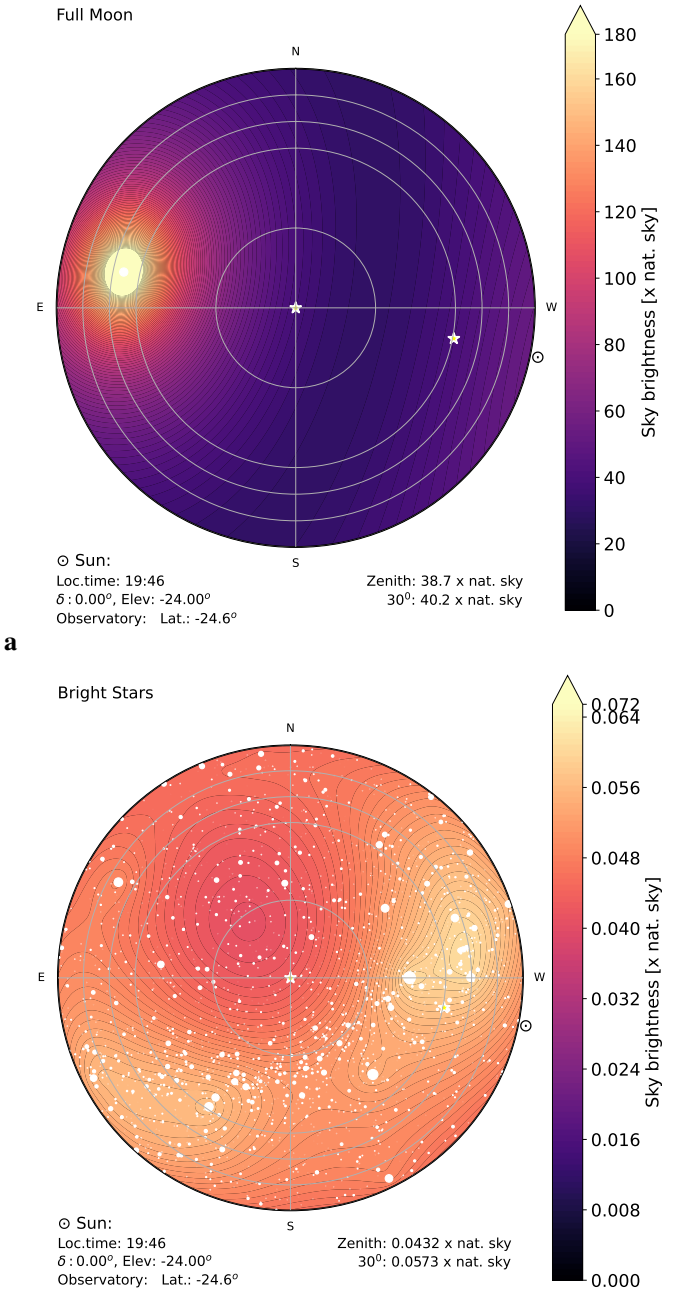

Fig. 2. Example of the scattered-light model for the full Moon (**a**) and for stars (**b**, marked by white dots scaled by magnitude), used for validation over the whole sky (see Fig. 1 for a general explanation of these figures). The colour scale is in nanolamberts in panel a and in fractions of the reference dark sky ($V = 22$ MpSA) in panel b.

Finally, satellites may be too faint to be detected as point sources or trails. In that case, they contribute to the sky background as a source of diffuse light. This is not relevant for images obtained with large telescopes, whose limiting magnitudes are much fainter than the effective magnitudes of all LEO satellites. For example, a combined 300-second exposure in the V band with FORS2, under median conditions, will result in a 5σ detection of an object with $V = 25.7$, while the faintest LEO satellite in our simulation (see Sect. 3.1) has $V_{\mathrm{eff}} = 11.6$: all satellites are

[4] PCmag.com, retrieved Feb. 2026
[5] `https://www.reflectorbital.com/`

detected as trails. It will, however, be relevant for some wide-field (e.g. all-sky) cameras or even for naked-eye observations. It is also critically relevant for observations with brighter limiting magnitudes, such as most spectroscopic observations (see Hainaut & Moehler 2024, for a discussion of the spectroscopic case).

We introduce a simple model of atmospheric scattering and validate it. We then use it to quantify the effect of existing and upcoming satellite constellations on the sky background via scattered and diffused light pollution and discuss the consequences.

2. Simulation methods

The evaluation of the scattered and diffuse light pollution, as well as the satellite densities, trail densities, and losses is computed using our Python implementation of the algorithm described in Bassa et al. (2022), expanded for this paper. The Python code and the accompanying configuration files are available on GitHub.[6]

2.1. Observatories and instruments

The simulations were performed for the FOcal Reducer/low dispersion Spectrograph 2 (FORS2; Appenzeller et al. 1998) in imaging mode. Typical combined exposures have a field of view (FoV) of $6 \times 6'$ for an exposure time of 300 s, with a limiting magnitude $V \sim 25.8$ (5σ). FORS2 is mounted on one of the 8.2-meter Unit Telescopes of ESO's Very Large Telescope, on Paranal, Chile (latitude 24.62° S). We used FORS2 as representative of traditional imaging cameras on large telescopes.

We also performed simulations for the NSF-DOE Vera C. Rubin Observatory Legacy Survey of Space and Time (LSST) camera. This camera combines a huge FoV of 3.5° diameter covered by 189 individual CCDs assembled in 21 rafts of 3×3 detectors. The camera is fed by the large, 8.4-meter diameter mirror of the telescope. Rubin observatory is located on Cerro Pachón, Chile (latitude 30.24° S). A typical 15-second exposure has a limiting magnitude $V \sim 24.9$ (5σ). The observatory is finalizing the commissioning of the system; it is likely that some of the operational parameters will change when in full operation. For instance, the exposure time increases from 15 to 30 s, which would double the counts from the following simulations. This combination makes the LSST a unique instrument in terms of sensitivity and FoV. These characteristics also make the LSST particularly sensitive to satellite trails. Furthermore, because of the high-density electronics required to control the CCDs, a satellite trail bright enough to saturate the detector will not only cause a broad trail but will also cause a series of parallel ghost trails resulting from cross-talk between the CCD controllers. These ghost trails appear in the affected CCD and in the other CCDs from the same raft, resulting in a dramatically multiplied loss of FoV. These effects are discussed in detail by Tyson et al. (2020). The potential of a satellite to trigger this cross-talk effect depends not only on its visual magnitude but also on its apparent angular velocity (a slower, higher satellite remains longer on a given pixel). It also depends on the apparent angular size of the satellite (a higher satellite will appear smaller, and its light will be concentrated on fewer pixels). Following Tyson et al. (2020), these parameters can be simplified to a threshold $V_{550\,\mathrm{km}} \leq 7$, which converts to an effective magnitude (accounting for trailing) $V_{\mathrm{eff}} \leq 18.3$ (see Bassa et al. 2022, for a discussion of the effective magnitude). This effect is one of the origins of the IAU recommendation $V_{550\,\mathrm{km}} > 7$; the other, $V > 7$, ensures that the satellites are not visible to the naked eye. The fact that the numerical values are equal is a welcome coincidence. We used the LSST camera as representative of the imaging cameras suffering from this type of effect (labelled as 'dramatic saturation'). Indeed, due to its large FoV on a large telescope, LSST is probably the instrument most sensitive to bright satellite trails.

Spectrographs, even mounted on very large telescopes, have much brighter limiting magnitudes. It is therefore common that a spectrograph does not register a satellite trail (see Hainaut & Moehler 2024, for a detailed discussion of the effects on spectrographs). In that case, the trail contributes to increasing the background; this is the 'diffuse light pollution'.

2.2. Observation geometry

For a satellite to affect the observations, it must be above the horizon and illuminated by the Sun. These conditions depend on the latitude of the observatory, the position of the Sun, and the position of the satellite. In the simulations described below, we used the position of the FORS2 and LSST instruments. We either scanned the full night or focused on the time when the Sun was at an elevation around −24°; this corresponds to ∼1h into the astronomical night and is therefore representative of near-twilight observations. Using the Bassa et al. (2022) method, we either scanned the whole sky, or focused on the zenith (the most favourable observing direction) and on a 30° elevation (corresponding to the typical limit for most observations) towards the direction of the Sun (where the number of illuminated satellites will be the highest), thereby bracketing most conditions.

2.3. Direct contamination

We first evaluated the direct effect of the satellites on the observations, as described in detail by Bassa et al. (2022). A rigorous quantification of the losses caused by satellite trails depends on the science case for which the data are acquired. For instance, in the case of a survey aiming at counting distant galaxies, the critical effect of satellite trails is to reduce the useful area of the FoV. In the case of targeted observations, however, a satellite trail missing the observed object might not be noticed directly but may affect the quality of the sky subtraction. To generalize the concept of data losses, we used the simple metric of the fraction of the FoV compromised by the trails. For this purpose, each trail was considered to cross the entire FoV, and its width was set to 5″, accounting for the intrinsic size of the satellite, the width of the point spread function (PSF) and its wings, including defocusing effects (see Tyson et al. 2020, for details) . To account for the wings of very bright satellite, this value was doubled for a satellite 100× brighter. We defined the loss metric as the total fraction of FoV caused by all the trails crossing an exposure. This neglects the superposition of trails and can result in a loss fraction larger than 100%, indicating that each pixel is on average affected by more than one trail. For the case of the LSST camera, we also account for the saturation effect described above.

2.4. Scattered light

We aimed to evaluate the contribution of scattered light from sources illuminating the atmosphere and to compare it to the optimal reference dark sky with $V = 22$ MpSA or

[6] SatConAnalytic package, `https://github.com/ohainaut/SatConAnalytic`

$L = 174$ μcd m^{-2} . We used the method described by Krisciunas & Schaefer (1991) (hereafter KS91) to evaluate the contribution of a satellite to the sky brightness. They developed this method to compute the contribution of the Moon to the sky brightness and validated it on 'a dozen of observations' of the moonlit sky over Mauna Kea. It also reproduces extensive measurements performed at Paranal well (Patat 2003). More detailed models of the Paranal night sky have been developed (Noll et al. 2012, e.g.); similarly, a much more advanced scattered-moonlight model is now available (Jones et al. 2013). However, the accuracy of the original KS91 method is sufficient for our purposes.

Following KS91 (their Eq. 15), the surface brightness (V) caused by the Moon is

$$V = f(\rho)\, I^*\, 10^{-0.4\, k\, X(Z_{\rm Source})} \left(1 - 10^{-0.4\, k\, X(Z)}\right), \quad (1)$$

where $f(\rho)$, the scattering function, is the intensity of the scattered light as a function of the scattering angle (ρ) between the line of sight and the source, $X(Z)$ is the length of the optical path in air masses (i.e. 1 at zenith) as a function of the zenith distance Z. The value $Z_{\rm Source}$ is the air mass of the source, i.e. the Moon, and Z is the air mass of the direction of observation. The value k represents atmospheric extinction in magnitudes per air mass. We used $k = 0.125$, corresponding to a typical value in the V band (see, for instance, the FORS2 data quality control[7]). The value I^* represents the illuminance of the source outside the atmosphere, so that the term $I^*\, 10^{-0.4\, k\, X(Z_{\rm Source})}$ represents the illuminance after atmospheric extinction.

For the air mass function, we used their Eq. 3:

$$X(Z) = \sqrt{1 - 0.96 \sin^2 Z}, \quad (2)$$

which they found to represent the scattering effect better than the simplified $X = \sec Z$ relation (valid only far from the horizon) as well as more complex relations used for photometric measurements very close to the horizon.

The scattering function $f(\rho)$ is the sum of the Rayleigh component $f_{\rm R}$ (caused by air molecules) and the Mie component $f_{\rm M}$ (accounting for atmospheric aerosols). For the Rayleigh scattering, they used

$$f_{\rm R}(\rho) = 10^{5.36} \left(1.06 + \cos^2 \rho\right), \quad (3)$$

and for the Mie scattering, they used

$$f_{\rm M}(\rho) = 10^{6.15 - \rho/40}, \quad (4)$$

where ρ is in degrees. The numerical factors were obtained empirically from their measurements, expressed in foot-candles (fc) for Moon illuminance and nanolamberts (nL) for the luminance. KS91 note that $f_{\rm M}$ was underestimated for $\rho < 10°$. As we are concerned with effects at large ρ, this is not an issue.

Combining Eqs. 1, 2, 3, and 4, we obtain the luminance (in nL) of the scattered light caused by a source with illuminance I (in fc). The transformations described in Appendix B convert between these non-standard units and standard photometric units.

To validate our implementation, we reproduced the surface brightness of the scattered moonlight, using $V = -12.74$ for the magnitude of the full Moon and setting the coordinates of the Moon directly opposite to the Sun. An example is displayed in Fig. 2.a. Both the spatial structure and the surface brightness of the moonlight are well reproduced, with $V \sim 18$ MpSA as expected.

To validate our model in the case of multiple sources, we computed the scattered light from stars. We used the stars from the Yale Bright Star Catalogue (HR; Hoffleit & Jaschek 1991) as sources and, for each star, computed its contribution to the scattered background. As the HR stars are limited to $V \leq 8$, this model lacks contribution from the numerous fainter stars. To correct for this, we computed a scaling factor using the magnitude distribution from Gaia DR3. Accounting for all stars down to $V \leq 21$, the flux from the HR stars must be multiplied by 2.2. An example is displayed in Fig. 2.b; far from the Milky Way, the scattered light represents 4% of the $V = 22$ MpSA dark sky, increasing to 6% in the Orion region (right part of the plot).

Equipped with the scattered-light model described above, we can now evaluate the contribution of satellites to the background sky. Each constellation is defined by a collection of shells, each described by an altitude, an orbital inclination, a number of planes, and a total number of satellites. For each constellation, the satellites were characterised by their standard magnitude at zenith at 550 km, $V_{550\ \rm km}$. The satellites were distributed among orbital planes and, within each plane, along the orbit. At any time, the positions of the satellites around the Earth were computed using simple Keplerian motion. The position of the Sun was computed for the time of observation, and the satellites in the shadow of the Earth were discarded. Similarly, the satellites below the observatory horizon were discarded. The coordinates of the remaining satellites were converted into topocentric azimuth and elevation. This simple mechanism aims to produce a representative distribution of the satellites in the sky, not to be ephemeris-accurate. Following Bassa et al. (2022), the magnitude of an illuminated satellite was simply scaled for its distance to the observer, without solar phase correction. For the Starlink satellites, this reproduces the observed magnitudes within ~ 1 mag, which is sufficient for our purposes (Bassa et al. 2022).

One issue with this method is that it relies on a single realisation of the satellite positions, which leads to local variations near individual satellites. A straightforward way to average out this effect would be to repeat the computation for several realisations and average the results. Instead, we worked with the apparent density of satellites (in satellites per square degree) computed analytically using the Bassa et al. (2022) method for each surface element of the sky. As demonstrated in that paper, this density is a rigorous average of the number of satellites in a given sky element over all possible realisations of their positions. The total flux reflected by the satellites was integrated over each element, yielding a total magnitude that was then used as input to the scattering model. An additional advantage of this approach is that the processing time is independent of the number of satellites (which is particularly beneficial when treating the mega-constellation of Sect. 3.2).

2.5. Diffuse light

A satellite can be too faint to be recorded as a trail, either because it is intrinsically too faint or because its apparent angular motion is too fast. In other words, its effective magnitude (see Bassa et al. 2022, for the detailed definition) is fainter than the limiting magnitude of the instrument. In that case, its light still contributes to the diffuse sky background. This effect is critical for very wide-angle systems, such as all-sky cameras or naked-eye observations, but also for most spectroscopic observations where the spectral dispersion of the light results in relatively bright limiting magnitudes (Hainaut & Moehler 2024).

[7] https://www.eso.org/observing/dfo/quality/FORS2/qc/photcoeff.html

The contribution of a constellation to the diffuse sky background was computed by integrating the flux from the satellites in a sky surface element. In turn, this was obtained by multiplying the satellite number density in that part of the sky by the angular area considered and by the flux corresponding to one satellite. This calculation was performed for each constellation shell to account for the different magnitudes of the satellites in different shells. The contributions of all shells were summed, resulting in the luminance of the sky surface element.

2.6. Simulated quantities and qualitative evaluation

For a given instrument, we set the observing conditions to a solar elevation $e_\odot = -21°$, i.e. 1.5 h after sunset (the actual time varies with the season and latitude), well into the astronomical night but at an instant when most of the satellites were still illuminated. The simulation was performed for the whole sky above the observatory, using the analytical method described in Bassa et al. (2022), resulting in a sky map like the example in Fig. 1. The values at zenith and at elevation $e = 30°$ (at the azimuth of the Sun) were recorded, corresponding to the range of elevations at which most observations were performed.

For critical cases, the simulation was repeated for solar elevations from 0° (sunset or sunrise) to −90° (nadir), corresponding to the full range accessible from Paranal Observatory.

The quantities computed are:

- satellite density, i.e. the number of satellites per square degree;
- number of trails crossing the instrument's FoV during an exposure;
- FoV losses, i.e. the average fraction of the FoV lost due to satellite trails. A value of 0.1, for instance, means that, on average, an exposure is crossed by trails damaging 10% of its pixels (not that one image in ten is lost while the others remain intact).
- diffuse light pollution, i.e. the contribution of satellites below the detection threshold to background brightness;
- scattered light pollution, i.e. the contribution of the scattered light from satellites to background brightness.

For the FoV losses (f), we set the following qualitative thresholds.

- Values $f < 0.3\%$ are considered 'good': the satellite-induced losses are in line with other losses affecting the data. The include bad columns on the detector, cosmic-ray hits, and bright-star spikes caused by diffraction on the telescope spider.
- Values $0.3 \leq f < 3\%$ are considered 'marginal'. On the VLT, the technical losses, caused by equipment failure, are at the $< 3\%$ level, which is considered a good trade-off between the cost of preventive maintenance (more of which could reduce technical losses) and residual losses. Three per cent is therefore the total acceptable losses budget.
- Values $3 \leq f < 30\%$ are considered 'bad', as this is significantly larger than the weather losses (typically $\sim 10\%$ for Paranal). At the 30% level, satellites would comprise, by far, the largest contribution to data losses.
- Values $f \geq 30\%$ are considered 'disastrous'. At that threshold, the production of data is severely compromised. In some cases, the losses can reach 100%, effectively rendering the telescope useless.

For sky-brightness pollution (p), the thresholds are as follows.

- Values $p < 0.5\%$ are flagged as 'good': the satellite-induced pollution is essentially negligible, well below the 1% limit for observatories.
- Values $0.5 \leq p < 10\%$ are considered 'marginal'. The light pollution remains below the IAU general recommendation for light pollution, but the sky is no longer 'observatory-grade'.
- Values $10 \leq p < 100\%$ are considered 'bad'. Observations are significantly affected: the faintest objects are no longer observable, and the exposure times required for the others increase by up to a factor of 2.
- Values $p \geq 100\%$ are considered 'disastrous': the light pollution is high enough to preclude deep, background-limited observations.

3. Simulation results

3.1. Upcoming constellations: Sixty-thousand satellites

We considered a set of five telecommunication constellations representing Starlink Gen. 1 and 2, OneWeb, GuoWang, and Amazon Leo (also known as Kuiper), with a total of over sixty-thousand satellites on 29 shells. This is the same configuration used by Bassa et al. (2022), detailed in their Table 1 and hereafter referred to as BHG2022 . While the actual architecture of each constellation is likely to evolve, this set is representative of the upcoming population of telecommunication satellites , with a mix of low- and high-altitude orbits from 328 to 1200 km. We set their absolute magnitudes to $V_{550\,\mathrm{km}} = 7$, which may be optimistic. This ensures that most satellites respect the IAU recommendation $V > 7$; the only exceptions are the few satellites on very low orbits, appearing close to zenith. Figure 3 displays the results; the values at zenith and at 30° elevation are listed in Table 1.

As discussed by Bassa et al. (2022), the fraction of FoV lost with this set of constellations is a fraction of a per cent in the regions of the sky where the satellites are illuminated, which dwindle about one hour after twilight. While this is an annoyance, that level of loss remains in the 'good' range. The diffuse light on all-sky cameras is of the order of $1–5 \times 10^{-4}$ times the natural sky background (i.e. negligible, in the 'good' range). Similarly, the scattered light is of the order of 10^{-4} times the natural sky (i.e. also negligible).

In summary, a sixty-thousand-satellite population, where all satellites adhere to the $V > 7$ limit, causes a non-zero but manageable effect on observations. Note, however, that some science cases may be more sensitive.

3.2. Mega-constellations: One million SpaceX orbital data centre satellites

We considered the SpaceX Orbital Data Center constellation, as described in McDowell's list[8], with a total of one million satellites. Of these, 500 000 are distributed on shells with altitudes between 400 and 1000 km, and the remaining 500 000 are distributed on sun-synchronous terminator orbits with altitudes between 700 and 1000 km to benefit from continuous illumination. The latter lie above the horizon only during twilight. To evaluate the impact of one million satellites, we spread the sun-synchronous satellites on a traditional Walker pattern. We set their absolute magnitudes to $V_{550\,\mathrm{km}} = 7$, which may be optimistic considering that the power requirements of these data centres require large solar panels and radiators. We therefore also

[8] Jonathan McDowell's constellation list, retrieved 2026-03-24

Table 1. Results of the simulations.

Constellation	N_{sat}	Mag $V_{550\ km}$	Satellite Density [sat/deg^2] Zenith	30°	Diffuse light pollution [fraction of dark sky] Zenith	30°	Scattered light pollution [fraction of dark sky] Zenith	30°	Fig.
Base scenario: Sixty-thousand satellites									
BHG2022	64 526	7	9.0×10^{-3}	0.053	3.4×10^{-4}	1.6×10^{-3}	1.1×10^{-4}	1.8×10^{-4}	3.acd
Mega-constellations									
SXODC-7	1M	7	0.58	1.6	5.8×10^{-3}	**0.015**	1.1×10^{-3}	1.5×10^{-3}	A.1.acd
SXODC-6	"	**6**	"	"	**0.015**	**0.038**	2.7×10^{-3}	3.8×10^{-3}	
SXODC-5	"	**5**	"	"	**0.037**	**0.095**	6.8×10^{-3}	9.4×10^{-3}	
Very bright satellites: Direct-to-cell									
AST	243	**2**	4.6×10^{-5}	2.6×10^{-4}	2.0×10^{-4}	3.3×10^{-4}	3.2×10^{-5}	4.7×10^{-5}	A.2.acd
D3000	3000	"	4.2×10^{-4}	2.4×10^{-3}	2.4×10^{-3}	3.9×10^{-3}	4.0×10^{-4}	5.6×10^{-4}	A.3.acd
Extremely bright satellites: Sunlight as a service									
RO-2027	36	**−4.3**	5.3×10^{-6}	3.2×10^{-5}	8.6×10^{-3}	**0.014**	1.9×10^{-3}	2.7×10^{-3}	8.a
RO-2030	5000	"	7.8×10^{-4}	4.6×10^{-3}	n/a		**0.27**	**0.37**	8.b
RO-2035	50 000	"	7.8×10^{-3}	0.046	n/a		**2.7**	**3.7**	8.c

Constellation	N_{sat}	Mag $V_{550\ km}$	Inst.	Trails per frame Zenith	30°	FoV loss [fraction of FoV] Zenith	30°	Fig.
Base scenario: Sixty-thousand satellites								
BHG2022	64 526	7	FORS	0.145	0.804	1.36×10^{-3}	5.98×10^{-3}	3.b
Mega-constellations								
SXODC-7	1M	7	FORS	4.27	11.5	**0.0593**	**0.160**	A.1.b
"	"	"	LSST	11.6	31.3	0.0108	0.0290	1
SXODC-6	"	**6**	"	"	"	**0.390**	**1.62**	5.a
SXODC-5	"	**5**	"	"	"	**11.6**	**19.5**	
Very bright satellites: Direct-to-cell								
AST	243	**2**	FORS	7.88×10^{-4}	2.54×10^{-3}	1.09×10^{-5}	3.52×10^{-5}	A.2.b
D3000	3000	**2**	FORS	8.19×10^{-3}	0.0265	1.14×10^{-4}	3.68×10^{-4}	A.3.b
"	"	"	LSST	0.0160	0.0614	0.0160	**0.0614**	6, A.4.d
Extremely bright satellites: Sunlight as a service								
RO-2027	36	**−4.3**	FORS	1.10×10^{-4}	3.65×10^{-4}	1.53×10^{-6}	5.06×10^{-6}	
			LSST	2.12×10^{-4}	8.30×10^{-4}	2.12×10^{-4}	8.30×10^{-4}	9.a
RO-2030	5000	"	FORS	0.0157	0.0518	2.18×10^{-4}	7.20×10^{-4}	
			LSST	0.0306	0.119	0.0306	**0.119**	9.b, 10.a
RO-2035	50 000	"	FORS	0.157	0.518	2.18×10^{-3}	7.20×10^{-3}	
			LSST	0.306	1.19	**0.306**	**1.19**	9.c, 10.b

Notes. All simulations were performed at solar elevation $e_\odot = -21°$, i.e. well into the astronomical night (e.g. ~ 1h40 after sunset for the VLT). **Constellations**: BHG2022: realistic upcoming set, from Bassa et al. (2022); see Sect. 3.1; SXODC: SpaceX Orbital Data Centre; see Sect. 3.2; AST: AST Space-Mobile; see Sect. 3.3; AST-3000 is an extrapolation of their proposed constellation; RO: Reflect Orbital, with the year of foreseen deployment; see Sect. 3.4. N_{sat} is the total number of satellites in the constellation. **Mag** is the magnitude of a satellite, reduced to a distance of 550 km. In the upper table: **Satellite density** is the average number of satellites per square degree. **Diffuse light pollution** is the contribution of the satellites to the sky background for instruments with a limiting magnitude brighter than the effective magnitude of the satellite (e.g. spectrographs). **Scattered light pollution** is the contribution of all the light from illuminated satellites, scattered (Mie and Rayleigh) by the atmosphere. Both types of pollution are given as a fraction of the dark sky (V = 22 MpSA, 174μcd m^{-2}). The lower table lists instrument-specific effects. **Inst.** specifies the instrument: FORS is a $6 \times 6'$ imager taking 300 s exposures, and LSST is a 3.9° camera taking 15 s exposures; see Sect. 2.1 for more details. **Trail per frame** gives the average number of detected satellite trails in an individual exposure. **FoV loss** refers to the average fraction of the FoV contaminated by the satellite trails. **Fig.** points to figures illustrating the values. The quantities are evaluated at zenith and at 30° elevation in the direction of the solar azimuth. These positions are marked by a star on the sky maps. The values in boldface are above the acceptable threshold (1% for light pollution, 3% for losses); the values in red lie above the disastrous threshold (10% for light pollution, 30% for losses).

considered $V_{550\ km}$ = 6 and 5. In the tables and figures, these constellations are labelled SXODC-7, -6, and -5.

The scattered light pollution (Fig. A.1.d) remains at the 0.1–0.2% level of the dark sky background (i.e. in the 'good' range), but the diffuse light pollution (Fig. A.1.c) is in the 0.5–1.5% range, i.e. above the 1% limit for prime astronomical sites. It is therefore flagged as 'marginal'.

Because of the large number of satellites, the number of trails per image increases dramatically compared to the previous section; consequently, the fraction of the FoV covered by trails also

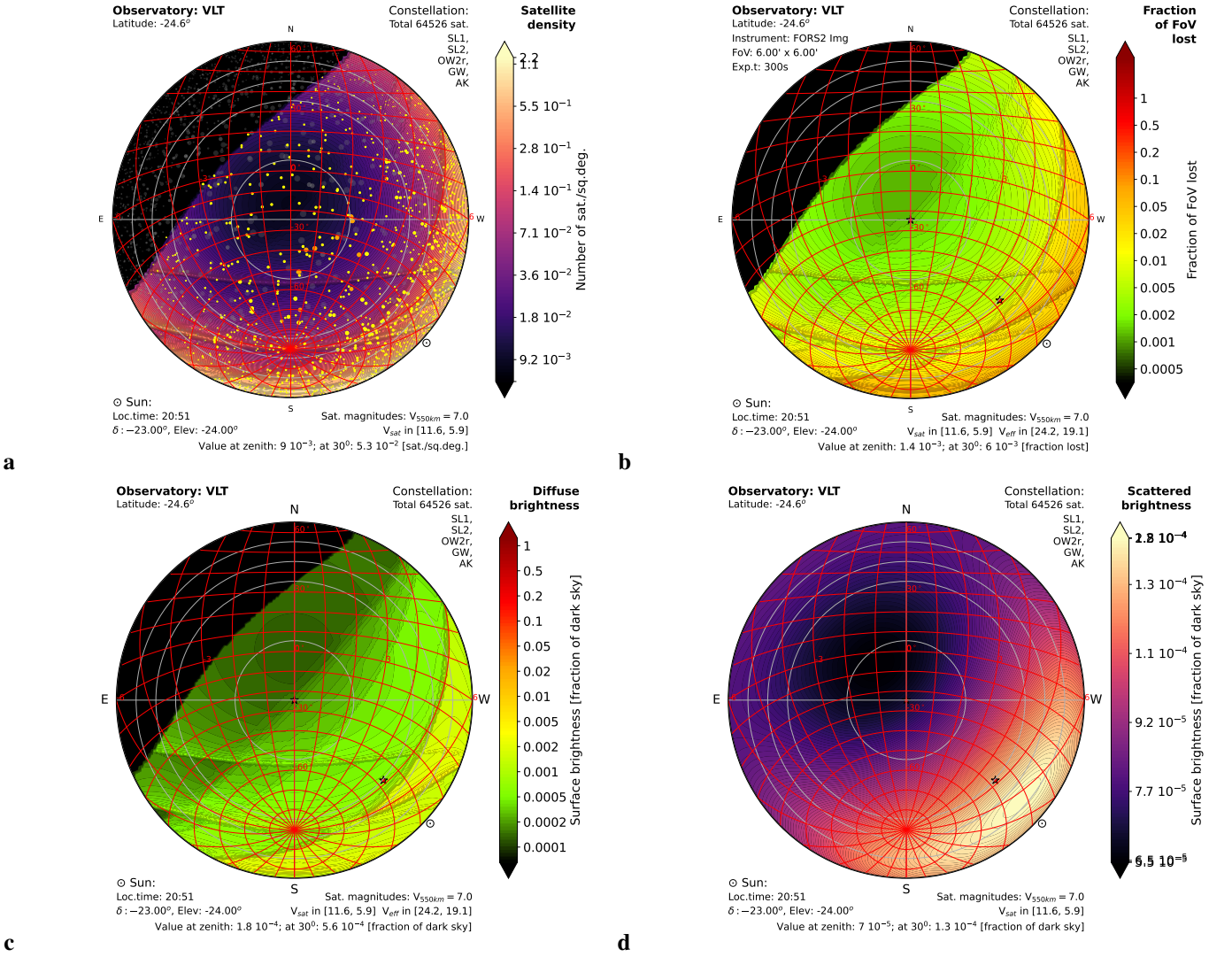

Fig. 3. For constellations with 64 526 satellites, representative of the near future (BHG2022 configuration): **a** Average satellite density [sat/sq. deg.]. The dots show an example of the satellite positions (grey for satellites in the Earth's shadow, yellow for illuminated satellites, and orange for satellites with $V < 7$). **b** Fraction of the FoV lost to satellite trails in 300-second ESO VLT FORS2 exposures. **c** Diffuse sky brightness – i.e. the direct contribution of all satellites to the background of instruments unable to detect the individual satellites – as a fraction of the natural dark sky with $V = 22$ MpSA. **d** Scattered sky brightness, including Mie and Rayleigh scattering from all illuminated satellites, as a fraction of the natural dark sky. A general description of these sky maps is given in Fig. 1.

increases dramatically. The example in Fig. A.1.d indicates that the losses will reach 6–15% (i.e. 'bad') when the Sun is at −24°. Figure 4 shows the evolution of the losses with solar elevation and local time, peaking at 28% when pointing towards the cusps of the constellation. These losses remain above the per cent level for most of the night, except when the Sun is below −60°, which occurs only during 2 h in spring or autumn nights and 4 h in winter nights — and not at all in summer. The example of FORS2 is representative of traditional imagers on large telescopes.

For a saturating detector such as the Rubin observatory's LSST, it is critical that the magnitudes of the satellites remain fainter than $V = 7$. Should the absolute magnitudes of the satellites reach $V_{550\ \mathrm{km}} = 6$, the effects would be devastating, as illustrated in Fig. 5.a. At $V_{550\ \mathrm{km}} = 5$, most of the LSST observations would be lost, firmly placing this scenario in the 'disastrous' regime. This sets stringent constraints on the satellite design, in terms of cross section and reflective properties, and on their operations, such as ensuring that they remain fainter than $V = 7$.

Additionally, because of the very large number of satellites, a minor violation of the $V_{550\ \mathrm{km}} > 7$ recommendation would result in many satellites becoming visible to the naked eye. For instance (see Fig. 5.b), should their $V_{550\ \mathrm{km}} = 5$, about 2000 satellites would be visible to the eye (brighter than $V = 7$) one hour after sunset. As a comparison, one can typically see four to five thousand stars. The satellites would significantly affect the appearance of the sky.

3.3. Very bright satellites: AST BlueBirds

Here, we discuss the case of the bright 'BlueBird' satellites by AST-SpaceMobile. Based on their website[9], the surface of these satellites will be 223 m^2. Using the measurements from Mallama & Cole (2025), i.e. $V_{550\ \mathrm{km}} = 2$, and a total number of 243 satellites (as in their petition to the Federal Communication Commission) on a set of realistic shells, we built the 'AST' con-

[9] https://ast-science.com

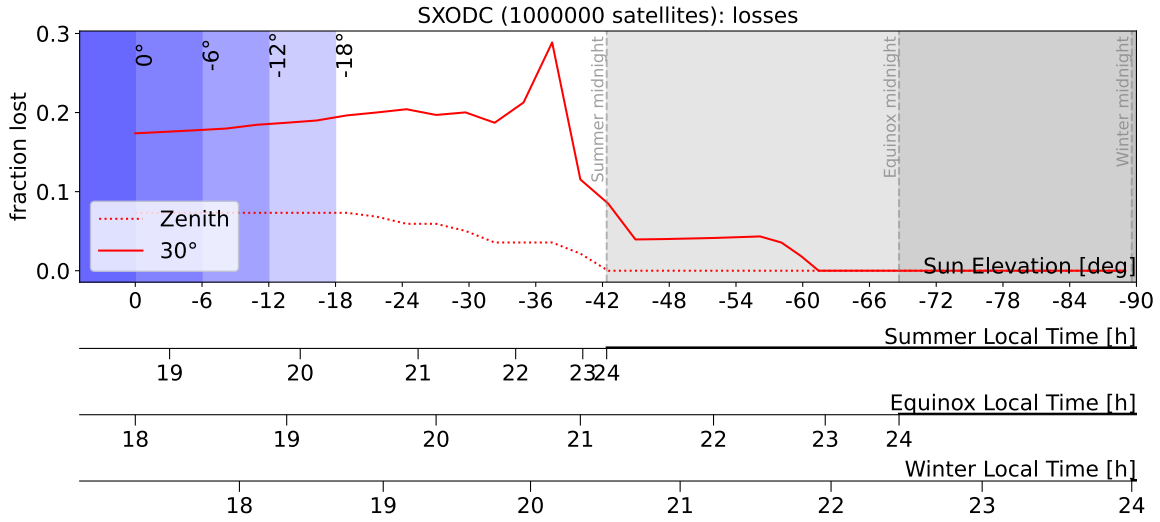

Fig. 4. For one million satellites ($V_{500\ \mathrm{km}} = 7$), representing the SpaceX Orbital Data Center constellation: Fraction of the FORS2 FoV lost as a function of solar elevation for observations at zenith and at 30° elevation towards the Sun. The peak at $\sim -36°$ corresponds to the time at which the measuring point crosses the cusp of the constellation. The secondary scales convert solar elevation into local solar time for the equinoxes and solstices. Twilights are shown in blue, and the inaccessible elevations in grey. Twilights are shaded in blue. The corresponding local times are given for the solstices and equinoxes, and the inaccessible elevations are shaded in grey. The corresponding sky maps are shown in Fig. A.1.

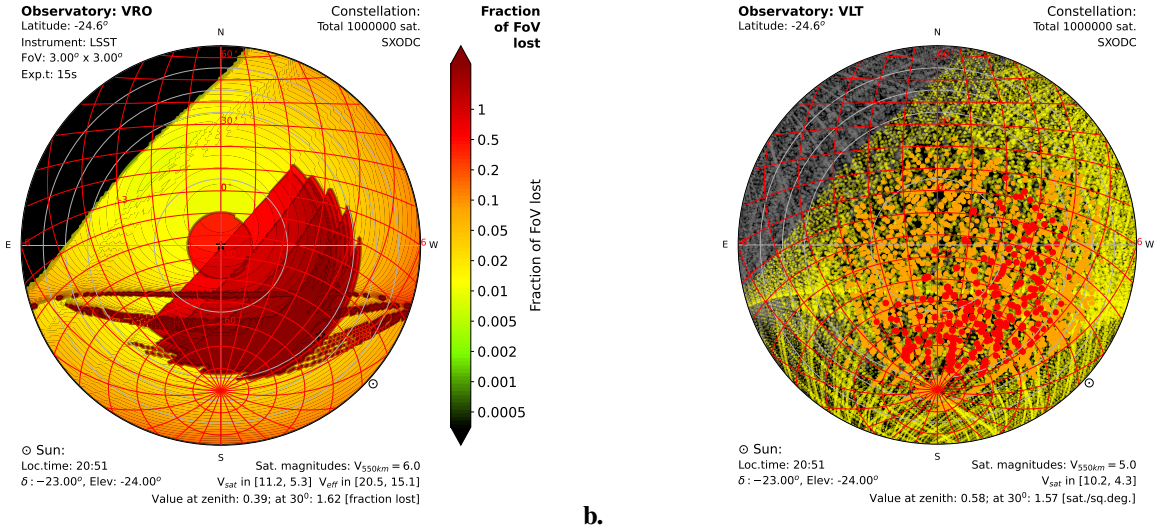

Fig. 5. For one million satellites ($V_{500\ \mathrm{km}} = 6$), representing the SpaceX Orbital Data Center constellation in slight violation of the $V > 7$ recommendation: **a.** Fraction of the FoV lost for the LSST camera. The values above 1 indicate that, on average, more than one satellite trail saturates a given pixel. The satellites' apparent angular velocity decreases at the constellation cusps, lowering their effective magnitudes and increasing their density. This results in higher losses in these regions. The red 'half circles' correspond to the lowest and brightest satellites, for which the Earth's shadow has already hidden part of the orbit. **b.** Example positions of the individual satellites. The grey dots represent invisible satellites in the Earth's shadow, whereas the coloured dots represent illuminated satellites. The 1867 orange dots correspond to satellites brighter than $V = 7$, and the 247 red dots to satellites brighter than $V = 5$. For comparison, about 3000–4000 stars are this bright (see Fig. 2.b).

stellation. To evaluate the effect of a larger constellation or the combination of various AST-like constellations, we also built a hypothetical constellation with 3000 BlueBird-like satellites on realistic orbits with altitudes ranging from 550 to 750 km; this hypothetical constellation is labelled 'D3000' (D stands for 'direct-to-cell').

In the case of the 300-satellite constellation, the small number of spacecraft ensures negligible losses on instruments not affected by saturation (Fig. A.2). In the case of the LSST camera, however, saturation drives the losses to 0.2–0.6% of the FoV, instead of 0.0002–0.0006% if the satellites had been fainter (see Fig. A.4.a and b). The effect on the sky-background pollution, both diffuse (at the 10^{-4} level) and scattered (at the 10^{-5} level), is negligible, as expected for a handful of illuminated satellites in the sky.

Even with 3000 bright satellites (Fig. A.3), the scattered light pollution remains negligible ($4–6 \times 10^{-4}$), while the diffuse light inches towards the tolerability limit of 1%: the pollution represents 0.2–0.4% of the dark sky. For non-saturating instruments, the FoV loss remains at the 10^{-4} level, still driven by the fairly small (compared to previous sections) number of satellites. For a saturating instrument such as the LSST, however, the losses be-

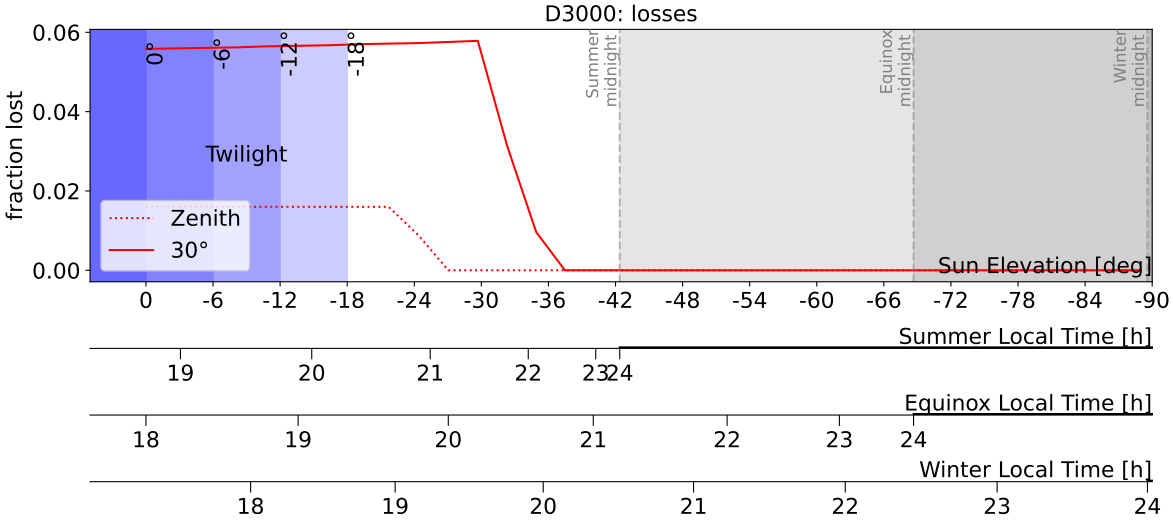

Fig. 6. FoV losses for a saturating camera, such as LSST, for constellations of 3000 BlueBird-like satellites representing a direct-to-cell constellation (code D3000 in the table), as a function of solar elevation. Twilights are shaded in blue. The corresponding local times are given for the solstices and equinoxes, while inaccessible elevations are shaded in grey.

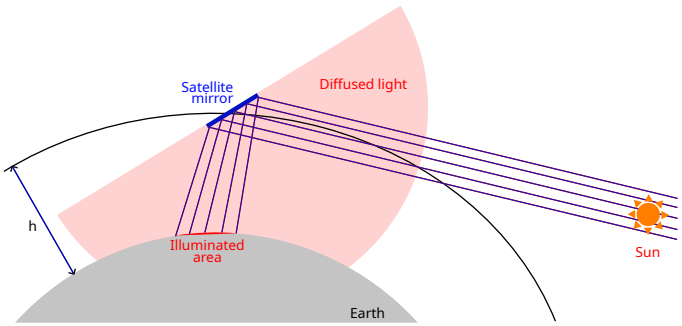

Fig. 7. Geometry of a large mirror-like satellite reflecting sunlight towards Earth. Part of the light is reflected onto a small area on the ground, while the remainder is diffused over a hemisphere. This illustration is not to scale.

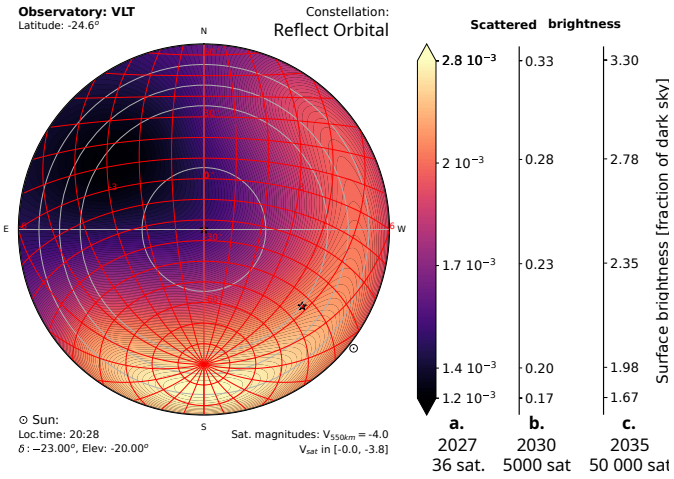

Fig. 8. Scattered light as a fraction of the natural dark sky for 37 (panel a), 5000 (b), and 50,000 (c) extremely bright satellites ($V_{500\ \mathrm{km}} = -4$), representing the Reflect Orbital constellations envisaged for 2027, 2030, and 2035, respectively, as seen from outside their illuminating beam. For more details, see Fig. 3.

come significant, in the 1–6% range (see Fig. 6). As in the case of the 243-satellite configuration, these losses are completely dominated by satellite brightness: had they respected the $V = 7$ limit, the losses would be at the 10^{-5} level (see Fig. A.4.c and d). All illuminated satellites (about 30–50 in the first and last hours of the night) would be clearly visible to the naked eye as bright sources, ranging from $V \sim 6$ close to the horizon to $V \sim 2$ close to zenith.

Overall, this experiment illustrates that satellites in a small to moderately sized constellation must still adhere to the $V > 7$ limit. Indeed, brighter satellites would have a disproportionate effect on saturating instruments as the LSST Camera.

3.4. Extremely bright satellites: Reflect Orbital sunlight as a service

In this section, we tackle the issue of extremely bright objects, such as the very large mirror-like satellites envisioned by Reflect Orbital[10]. They plan[11] to launch a single prototype satellite in 2026, soon followed by a modest constellation of 36 satellites in 2027 and a production constellation of 5000 satellites in 2030. They also mention an extension to 50 000 satellites by 2035. In the table and figures, these are labelled RO-2027, RO-2030, and RO-2035. The company has not made their constellation architecture available, so we distributed the satellites over three Walker shells with altitudes between 600 and 650 km on orbits at an arbitrary but realistic inclination of 55°. For the simulation of the various effects on observations, we assumed that no satellite points its reflected beam to or near the observatory and that all illuminated satellites are in an operational attitude.

To estimate the magnitude of these objects, we considered the mirror area. It is suggested that a Reflect Orbital satellite could be $57 \times 57 \sim 3\,000$ m^2. Following the simple geometry illustrated in Fig. 7, the mirror is illuminated by the Sun, with an illuminance $V = -26.75$, or $I = 127\,000$ lx $= 164$ W m^{-2}in the

[10] https://www.reflectorbital.com/
[11] https://www.reflectorbital.com

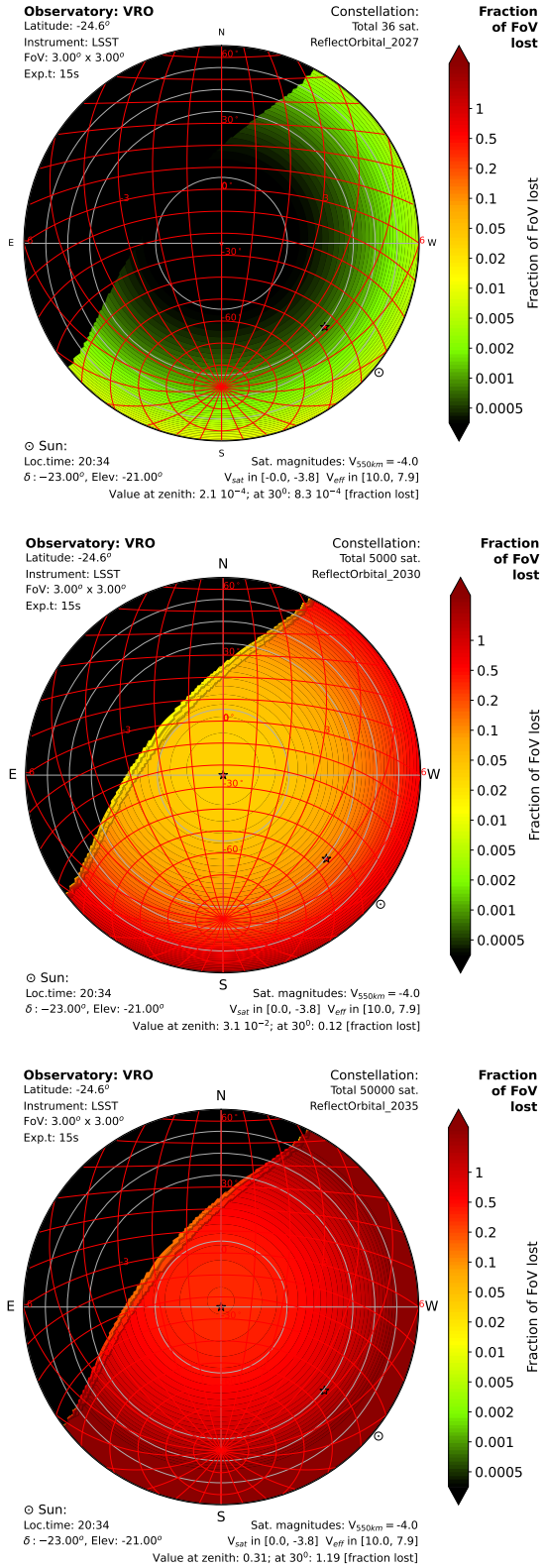

Fig. 9. Fraction of exposure lost for an instrument such as the LSST Camera for 36 (**a**), 5000 (**b**), and 50 000 (**c**) extremely bright satellites ($V_{500\ \mathrm{km}} = -4$), representing the Reflect Orbital constellations envisaged for 2027, 2030, and 2035, respectively, as seen from outside their illuminating beam. A loss greater than 1 means that, on average, each pixel is affected by more than one satellite trail. For more details on these sky maps, see Fig. 3.

V band. Assuming the mirror is oriented at 45° with respect to the incident light, it collects $F \sim 348$ kW. A fraction R of that light is reflected towards the Earth, and the remainder is diffused over half a sphere. Formally, part of it is also absorbed. However, assuming that the reflector is made of high-reflectivity coated Mylar, we neglect the absorption.

The diffused light, $(1 - R)\ F$, is spread over 2π sr. A unit area on the ground subtends $1/h^2$ sr, with $h = 550$ km being the altitude of the satellites. This results in the diffused-light illuminance $I_{\mathrm{diff}} = (1 - R)I/(2\pi h^2)$ at zenith.

The fraction of reflected to diffused light, R, is difficult to estimate. For a carefully optimised dielectric film, SpaceX (2022) obtain a ratio of 10^7 between the reflected and diffused illuminances. An earlier version of the film resulted in a ratio of 10^5. While a Mylar sheet is likely to also have a very high ratio, it is expected that the unfurling of the mirror will leave some small- and large-scale irregularities. Furthermore, the mirror is expected to degrade with time, resulting in less light being reflected in the main beam. Setting $R = 0.1$, we obtain a ratio of 9×10^{-5} between the diffused and reflected illuminances, which results in

- illuminance in the reflected beam $I = 1.8 \times 10^{-3}$W m^{-2}= 1.4 lx or $V = -14.3$. This is ~ 4 times brighter than the full moon, and the illuminance produced agrees with that listed in Reflect Orbital's web page.
- diffuse illuminance outside the beam $I_{\mathrm{diff}} = 1.7 \times 10^{-7}$W m^{-2}= 1.3×10^{-4} lx or $V_{\mathrm{diff}} = -4.3$, i.e. close to the maximum brightness of Venus.

Because of the modest number of satellites (compared to those in Sect. 3.1 and 3.2), the direct losses caused by satellite trails on the data will be small for instruments not suffering from saturation. For the saturating LSST Camera, however, the effects of even a single satellite crossing its FoV will be devastating (Tyson et al. 2020), compromising a very high fraction of the frame affected by that single trail, as illustrated in Fig. 9. The 2030 constellation (5000 satellites) would ruin 3% (at zenith) to 12% (at 30° elevation) of the LSST FoV one hour after sunset. With the 2035 constellation (50,000 satellites), the losses would be catastrophic, about 30% at zenith to 100% at 30°: all LSST images would be entirely unusable.

Clearly, all the illuminated satellites are visible as objects brighter (with V in the −4 to 0 range) than the brightest stars. With 5000 satellites, one can expect $\sim$ 130 Venus-bright satellites, and with a 50 000-satellite constellation, about 1300 Venus-like satellites criss-cross the sky. Furthermore, those directly illuminating the observer appear as points brighter than the full Moon, which have no natural equivalent.

These satellites are so bright that most instruments will detect them directly. Only for long exposures with high-resolution spectrographs will their effective magnitudes be fainter than the instrument's limiting magnitude. In that case, the test constellations with 37, 5000, and 50,000 satellites would increases the sky background by factors of 0.09, 0.7, and 7, respectively, relative to the dark sky background.

In terms of scattered light, only the smallest, 36-satellite constellation contributes an acceptable level of light pollution (0.15 to 0.21% of the dark sky; see Fig. 8a). With 5000 satellites, the pollution reaches 20 to 30% (Fig. 8.b), corresponding to an increase in exposure times by the same amount. The sky brightnesses would be $V = 21.8$ to 21.7 MpSA, or Bortle Class 2. Finally, with 50 000 satellites, the scattered light pollution will reach 2 to 3× the dark sky, i.e. increasing the total sky brightness by a factor 3 to 4. This corresponds to $V = 20.8$ to 20.5 MpSA

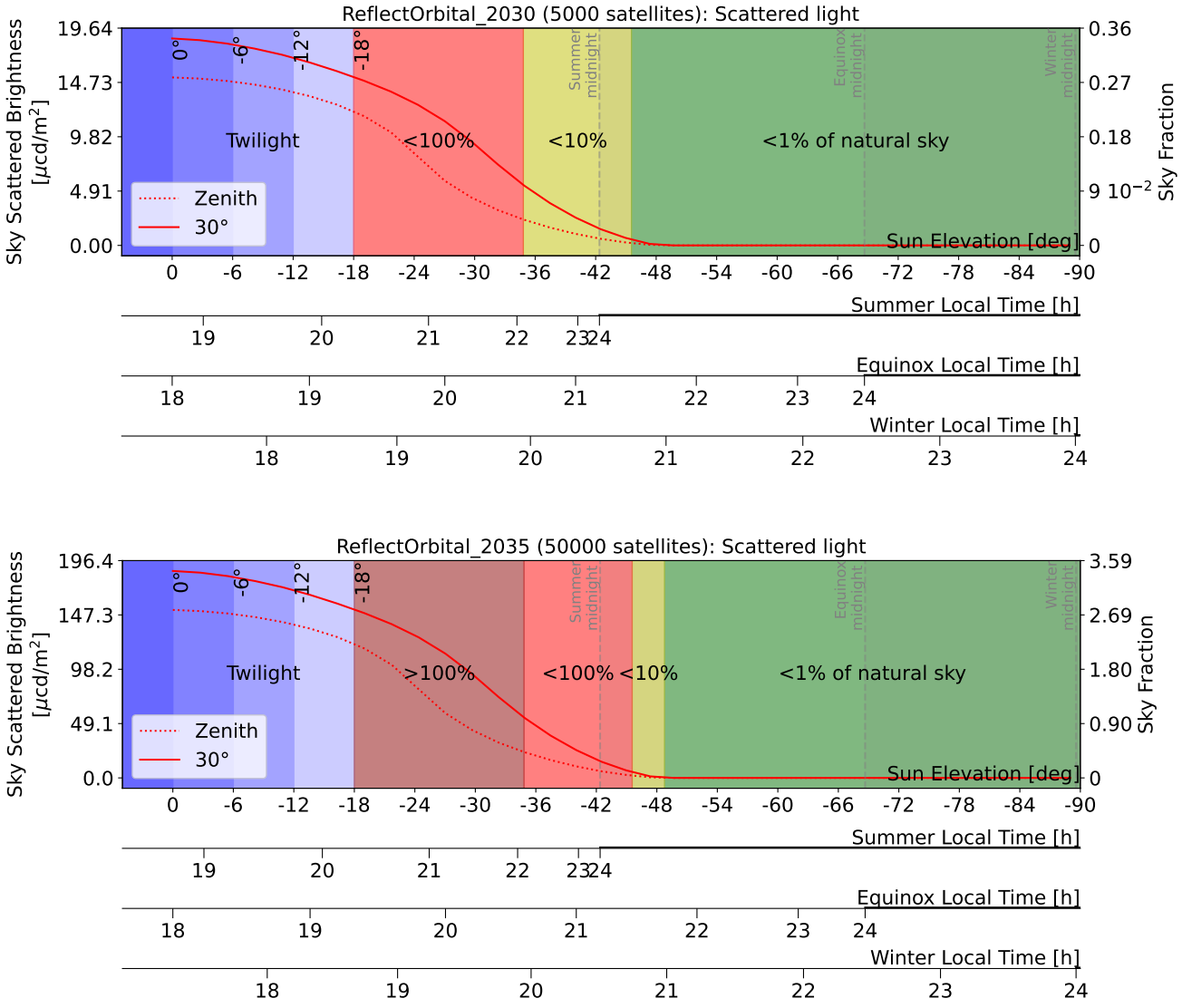

Fig. 10. Evolution of scattered light as a function of solar elevation for 5000 (a) and 50,000 (b) extremely bright satellites ($V_{500\ km} = -4$), representing the Reflect Orbital constellations envisaged for 2030 and 2035, respectively, as seen from outside their illuminating beam. Twilights are shaded in blue. The corresponding local times are given for the solstices and equinoxes, while inaccessible elevations are shaded in grey. Observing conditions remain good when pollution is < 1% of the natural sky (green shading). They are compromised when pollution ranges from 1 to 10% (yellow), jeopardised between 10 and 100% (red), and impossible above 100% (dark red).

and would push a prime site to Bortle Class 4.5, that is 'semi-suburban', unsuitable for dark-time astronomical observations.

Figure 10 displays the evolution of the scattered light pollution with the elevation of the Sun for the 5000 and 50,000 satellites, showing that good observing conditions (< 1% pollution) can be preserved only when the Sun is below −48° elevation. Accounting for seasonal changes, this geometry does not occur at all on summer nights, which are then 100% compromised. Around the equinoxes, ∼ 47% of the night is compromised, and during the winter, ∼ 40% of the night is compromised. It is important to note that the change from 5000 to 50,000 satellites does not change these 1% pollution limits significantly, but it increases the fraction of the night during which the pollution is above 10% of the dark sky.

3.5. Generalization

The previous sections, in which we evaluated in detail the effects of a series of constellations being considered for launch and operations, have revealed the importance of two main parameters: the total number of satellites and their magnitude $V_{550\ km}$. To characterize this dependence, we used the constellation from Sect. 3.1, with a realistic distribution of altitudes and inclinations. This constellation was scaled for a total number of satellites in the 10^2 to 10^6 range and for $V_{550\ km}$ in the range from −4 (corresponding to the brightest objects in this study) to 7 (the IAU recommendation). Figure 11 displays the results.

To keep the light pollution below the 1% limit, the total number of satellites must remain below ∼ 1000 for $V_{550\ km} = 2$ and below a few tens for $V_{550\ km} = -4$. To keep the direct FoV losses below the technical downtime, the total number of satellites with $V_{550\ km} = 7$ must remain below ∼ 10^5. Brighter satellites, even

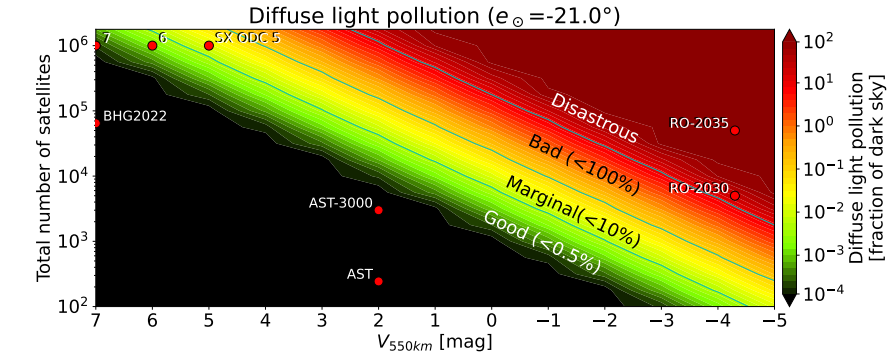

a

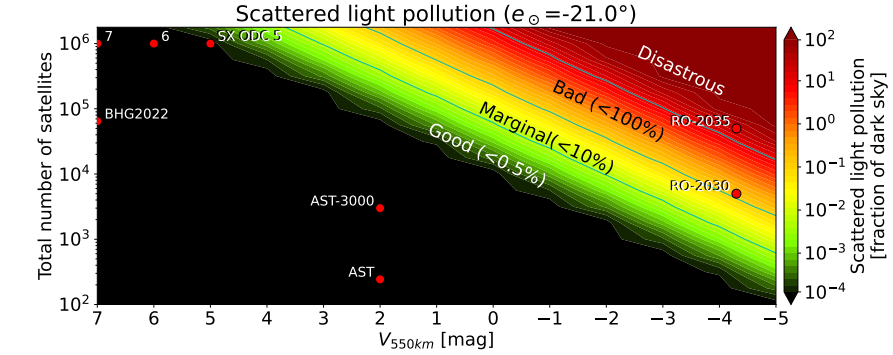

b

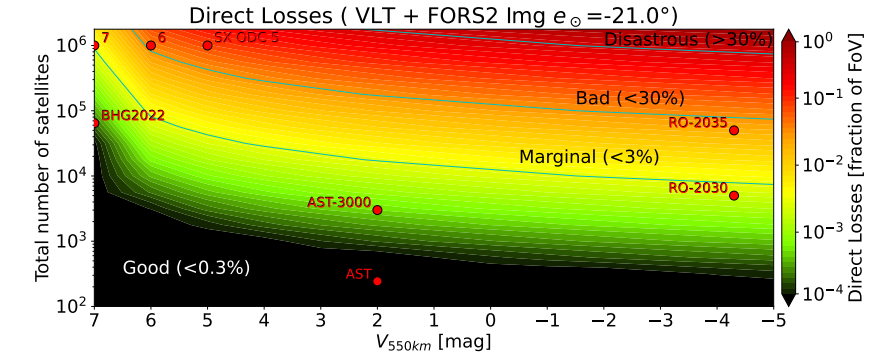

c

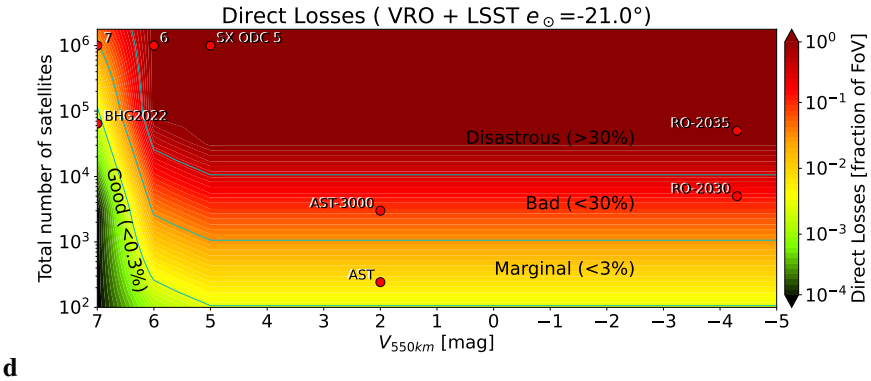

d

Fig. 11. Diffuse (**a**) and scattered (**b**) light pollution and FoV losses for FORS2 (**c**, a traditional imaging camera), and LSST (**d**, a saturating camera) as functions of the total number of satellites in orbit and their $V_{550\ \mathrm{km}}$. The light-pollution thresholds are 0.5% (below the limit for an observatory), 10% (generic IAU limit), and 100%. The loss thresholds are 0.3% (corresponding to one tenth of the technical losses), 3% (equal to the technical losses), and 30% (about 2–3× the technical and weather losses). The various constellations studied in this paper are indicated as dots.

marginally, have a dramatic effect on the FoV losses for saturating instruments: just 2000 satellites with $V_{550\ \mathrm{km}} \leq 6$ would degrade the performance of the LSST camera by 3%, and 20 000 by 30%.

Constellation effects are cumulative. It is therefore absolutely critical to account for the total number of satellites in orbit.

4. Discussion and conclusions

We evaluated the impact of a range of plausible and proposed satellite constellations on astronomical observations. Two representative instruments were chosen: FORS2 on ESO's VLT (a traditional imager on a large telescope) and the LSST camera at the Rubin observatory (an archetype of saturating instruments that suffer cross-talk damage when bright satellites cross the detector). The number of illuminated satellites depends on solar

elevation ($e_\odot$) below the horizon, which varies with local time and season. We therefore adopted $e_\odot = -20°$ to $-24°$ as representative dark-time conditions. For critical cases, we also covered the full range from $e_\odot = 0°$ (sunset or sunrise) to $-90°$ (nadir, in winter). All values were evaluated at zenith and at 30° elevation, covering the practical range of most astronomical observations. Constellation architectures were taken from publicly available information when possible; otherwise, standard, realistic assumptions were assumed.

We estimated the resulting losses using the analytical method of Bassa et al. (2022), extended here to include diffuse light pollution (the contribution from satellites too faint to be detected as trails) and scattered light pollution (including Mie and Rayleigh scattering from all illuminated satellites). The Python code used for these calculations is publicly available on GitHub, and the relevant photometric and radiometric conversions are summarized in Appendix B.

Our results lead to the following main conclusions about bright or very bright satellites (i.e. those with $V_{550\,\mathrm{km}} << 7$):

- Bright satellites cause dramatic FoV losses for saturating instruments. Constellations that do not respect the $V_{550\,\mathrm{km}} > 7$ limit significantly degrade the performance of saturating instruments such as the Rubin Observatory LSST camera, which suffers from saturation cross-talk, because of satellite brightness, the sheer number of satellites, or both.
- Bright satellites would dramatically affect the appearance of the night sky. A large constellation such as SpaceX's Orbital Data Center with $V_{550\,\mathrm{km}} = 5$ would place thousands of satellites above naked-eye visibility – comparable to the number of natural stars visible in a dark sky. AST SpaceMobile would add tens of bright objects ($V \sim 6$ to 2), while Reflect Orbital would produce more than 100 Venus-bright satellites by 2030 and over 1000 by 2035 (excluding direct beams to observers). In light-polluted regions, one could effectively see only artificial satellites at night.
- Very bright satellites affect the sky background. Large (60,000) to very large (one million) constellations adhering to the $V_{550\,\mathrm{km}} > 7$ limit have negligible to modest effects on sky-background pollution. Reflect Orbital, by contrast, presents a severe case: its 2030 constellation of 5000 very bright satellites would add scattered light equal to 20%–30% of the natural sky background (V = 21.8–21.7 MpSA). The 2035 configuration with 50,000 satellites would increase background by 200%–300%, reaching V = 20.8–20.5 MpSA—roughly corresponding to a semi-suburban Bortle Class and unsuitable for dark-time observations.

The number of satellites also matters, even when they satisfy the $V_{550\,\mathrm{km}} \geq 7$ recommendation:

- A ∼60 000-satellite set is manageable in terms of FoV losses (below the 1% level).
- A mega-constellation of one million or more satellites would fundamentally alter observing conditions. Most exposures would contain multiple trails throughout a large fraction of the night, with FoV losses rising to 10%–20%—making satellites the dominant data-loss source, exceeding weather and technical downtime.

Using the Bassa et al. (2022) constellation set, we generalized these results as functions of both satellite brightness and total constellation size. Since effects are cumulative, the total in-orbit population is the key parameter. For satellites satisfying $V_{550\,\mathrm{km}} > 7$, the total must remain below ∼100,000 to keep FoV losses within technical-downtime levels. Slightly brighter satellites ($V_{550\,\mathrm{km}} \leq 6$) degrade performance rapidly: just 2000 would cause 3% LSST losses, while 20,000 would reach 30%. For $V_{550\,\mathrm{km}} \leq 5$, only a few hundred satellites are tolerable if cross-talk losses are to remain below technical downtime.

The collection of constellations currently proposed for launch and operation considers over 1 700 000 satellites, many of which are brighter than, or significantly brighter than $V_{550\,\mathrm{km}} = 7$. This would have a devastating impact on astronomical observations.

This study focused on optical astronomy: direct effects of satellite trails crossing the FoV and indirect effects from diffuse and scattered light pollution. Satellite constellations also affect radio and millimetre observations. Beyond astronomy, they raise concerns about orbital crowding, space debris, and atmospheric pollution from launches and re-entries. These broader issues deserve attention but lie beyond this paper's scope.

Acknowledgements. This paper has been reviewed by two anonymous referees from the International Astronomical Union (IAU) Centre for the Protection of the Dark and Quiet Sky (CPS[12]). The author is grateful for their constructive comments. The author is also grateful to B. M. Kioko (ESO), J. C. Barentine (Dark Sky Consulting), and C. Walker (IAU CPS) for their helpful discussions and comments on the manuscript. Our SatConAnalytic python package relies on NumPy[13] (Harris et al. 2020), Matplotlib[14] (Hunter 2007), and Astropy[15] (Astropy Collaboration et al. 2013, 2018, 2022), a community-developed core Python package for Astronomy. This paper used data from the 2008 Whole Heliosphere Interval (WHI) Solar Irradiance Reference Spectra (SIRS) described in Woods et al. 2009 (https://doi.org/10.1029/2008GL036373). These data were accessed via the LASP Interactive Solar Irradiance Datacenter (LISIRD) (https://lasp.colorado.edu/lisird/).

References

Appenzeller, I., Fricke, K., Fürtig, W., et al. 1998, The Messenger, 94, 1
Astropy Collaboration, Price-Whelan, A. M., Lim, P. L., et al. 2022, ApJ, 935, 167
Astropy Collaboration, Price-Whelan, A. M., Sipőcz, B. M., et al. 2018, AJ, 156, 123
Astropy Collaboration, Robitaille, T. P., Tollerud, E. J., et al. 2013, A&A, 558, A33
Bará, S. 2019, Photonic Lett. of Poland, 11, 63
Bará, S., Aubé, M., Barentine, J., & Zamorano, J. 2020, MNRAS, 493, 2429
Barentine, J. 2025, Zenodo, Artificial Light at Night: State of the Science 2025 https://doi.org/10.5281/zenodo.15492393
Barentine, J. C. 2022, Nature Astronomy, 6, 1120
Bassa, C. G., Hainaut, O. R., & Galadí-Enríquez, D. 2022, A&A, 657, A75
Blanton, M. R. & Roweis, S. 2007, AJ, 133, 734
Boley, A. C., Green, R., Rawls, M. L., & Eggl, S. 2025, Research Notes of the American Astronomical Society, 9, 60
Bortle, J. E. 2001, S&T, 101, 126
Chen, X., Gu, H., Wang, C., et al. 2025, PASP, 137, 094504
Cinzano, P., Falchi, F., & Elvidge, C. D. 2001, MNRAS, 328, 689
Cole, R. E., Mallama, A., Harrington, S., & Respler, J. 2025, arXiv e-prints, arXiv:2505.05820
Cox, A. N. 2000, Allen's astrophysical quantities
Hainaut, O. R. & Moehler, S. 2024, A&A, 683, A147
Hainaut, O. R. & Williams, A. P. 2020, A&A, 636, A121
Hall, J., Walker, C., Rawls, M., et al. 2021, in Bulletin of the American Astronomical Society, 2.205
Harris, C. R., Millman, K. J., van der Walt, S. J., et al. 2020, Nature, 585, 357
Hasan, I., Tyson, J. A., Saunders, C., & Xin, B. 2022, Astronomy and Computing, 39, 100584
Hipparchus. 120BC, Hipparchi Bithyni In Arati et Eudoxi Phaenomena (Nicaea)
Hoffleit, D. & Jaschek, C. 1991, The Bright star catalogue (Yale University Observatory)
Hunter, J. D. 2007, Computing in Science & Engineering, 9, 90

[12] https://cps.iau.org
[13] https://numpy.org/
[14] https://matplotlib.org/
[15] https://www.astropy.org/

IAU-CPS, Gyula I. G. Józsa, Andrew Williams, et al. 2024, arXiv e-prints, arXiv:2412.08244
Johnson, H. L. & Morgan, W. W. 1953, ApJ, 117, 313
Jones, A., Noll, S., Kausch, W., Szyszka, C., & Kimeswenger, S. 2013, A&A, 560, A91
Kocifaj, M., Kundracik, F., Barentine, J. C., & Bará, S. 2021, MNRAS, 504, L40
Krisciunas, K. & Schaefer, B. E. 1991, PASP, 103, 1033
Lawrence, A., Rawls, M. L., Jah, M., et al. 2022, Nature Astronomy, 6, 428
Leinert, C., Bowyer, S., Haikala, L. K., et al. 1998, A&AS, 127, 1
Mallama, A. & Cole, R. E. 2025, MNRAS, 544, L15
Mallama, A., Cole, R. E., Harrington, S., & Maley, P. D. 2022, arXiv e-prints, arXiv:2211.09811
Masana, E., Carrasco, J. M., Bará, S., & Ribas, S. J. 2021, MNRAS, 501, 5443
McDowell, J. C. 2020, ApJ, 892, L36
Noll, S., Kausch, W., Barden, M., et al. 2012, A&A, 543, A92
Patat, F. 2003, A&A, 400, 1183
SpaceX. 2022, Brightness Mitigation Best Practice for Satellite Operators, Tech. rep., SpaceX, "Brightness Mitigation Best Practice for Satellite Operators" https://api.starlink.com/public-files/BrightnessMitigationBestPracticesSatelliteOperators.pdf
Stoppa, F., Groot, P. J., Stuik, R., et al. 2024, A&A, 692, A199
Tyson, J. A., Ivezić, Ž., Bradshaw, A., et al. 2020, AJ, 160, 226
Walker, C., Di Pippo, S., Aubé, M., et al. 2021, Dark & Quiet Skies II (2021), Dark & Quiet Skies II (2021), Report of the conference held 3-7 October, 2021.
Walker, C., Di Pippo, S., Aubé, M., et al. 2020, Dark & Quiet Skies I (2020), Dark & Quiet Skies I (2020), Report of the conference held 5-9 October, 2020.
Walker, C., Hall, J., Allen, L., et al. 2020, SatCon1: Impact of Satellite Constellations on Optical Astronomy and Recommendations Towards Migigations
Woods, T. N., Chamberlin, P. C., Harder, J. W., et al. 2009, Geophys. Res. Lett., 36, L01101

Appendix A: Figure set

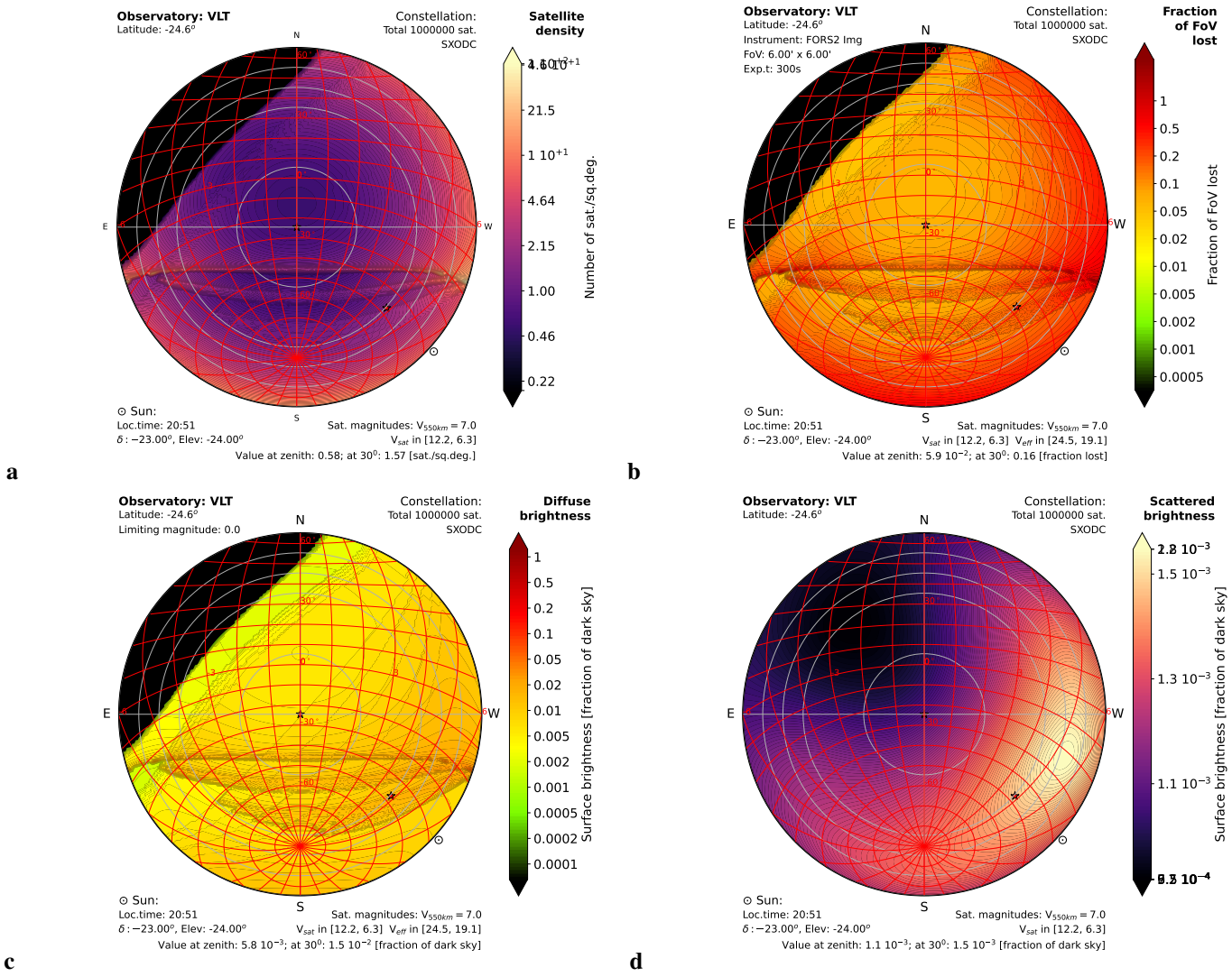

Fig. A.1. For one million satellites ($V_{500\ \mathrm{km}} = 7$), representing the SpaceX Orbital Data Center constellation: **a** Average satellite density [sat/sq. deg.]. **b** Fraction of the FoV lost to satellite trails in 300-second FORS2 exposures. **c** Diffuse sky brightness as a fraction of the natural dark sky with $V = 22$ MpSA. **d** Scattered sky brightness as a fraction of the natural dark sky. See Fig. 1 for a general description of the sky maps.

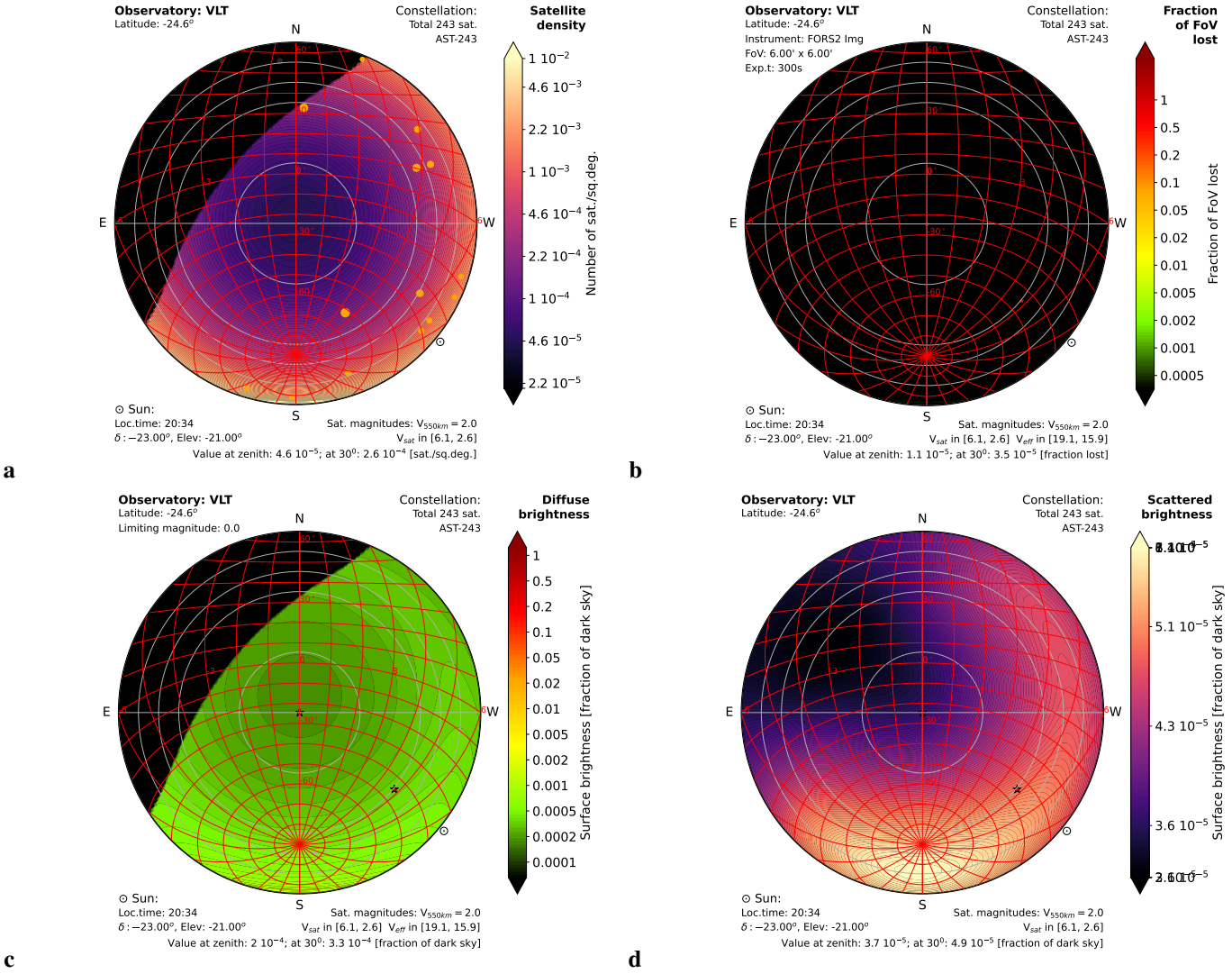

Fig. A.2. For 243 bright satellites ($V_{500\ \mathrm{km}} = 2$), representing BlueBird-like spacecraft in a constellation such as AST SpaceMobile: **a** Average satellite density [sat/sq. deg.]. **b** Fraction of the FoV lost to satellite trails in 15-second LSST exposures. **c** Diffuse sky brightness as a fraction of the natural dark sky with $V = 22$ MpSA. **d** Scattered sky brightness as a fraction of the natural dark sky. For more details, see Fig. 3.

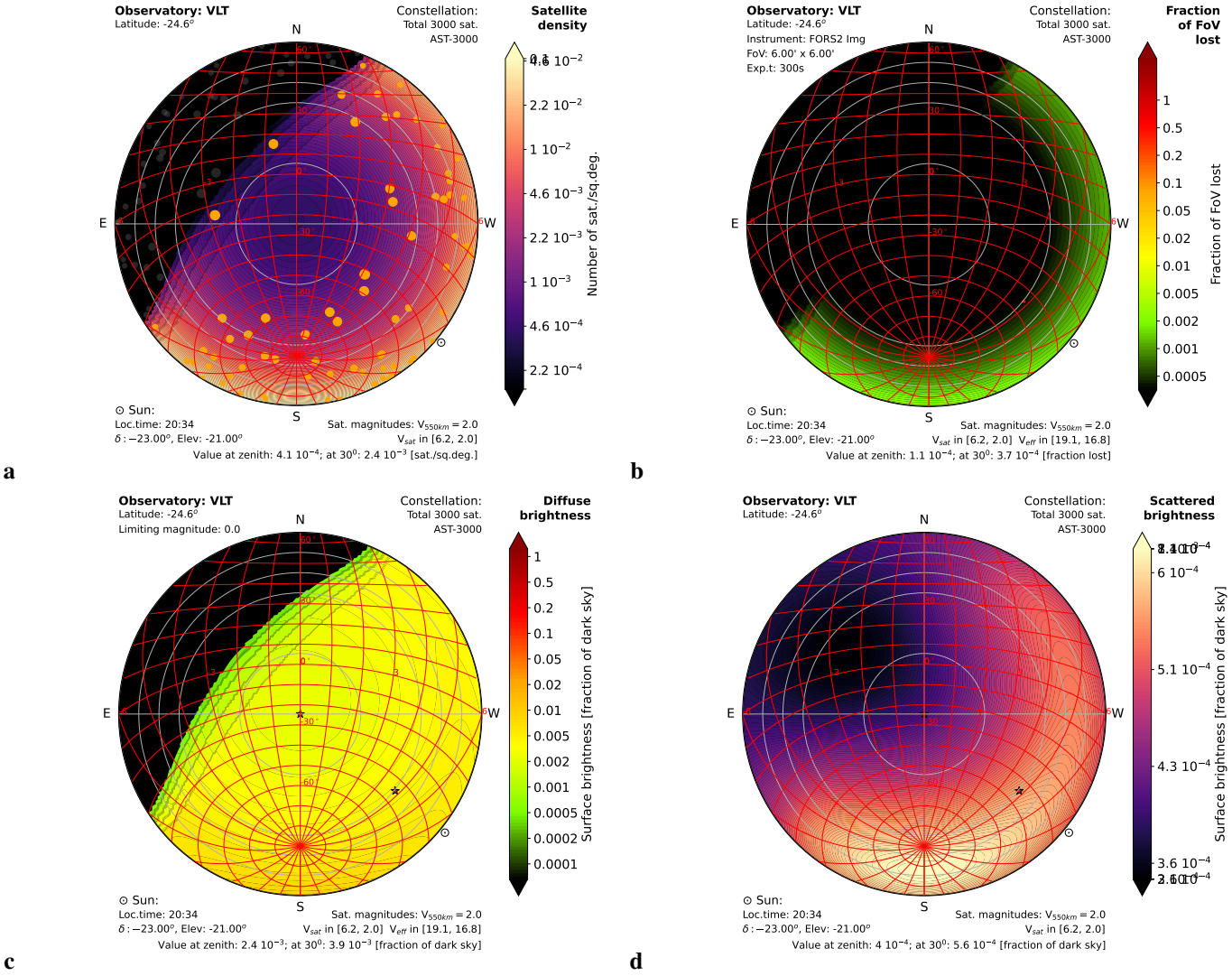

Fig. A.3. For 3000 bright satellites ($V_{500\ \mathrm{km}} = 2$), representing BlueBird-like spacecraft in a direct-to-cell constellation (code D3000 in the table): **a** Average satellite density [sat/sq. deg.]. **b** Fraction of the FoV lost to satellite trails in 15-second LSST exposures. **c** Diffuse sky brightness, as a fraction of the natural dark sky with $V = 22$ MpSA. **d** Scattered sky brightness, as a fraction of the natural dark sky. For more details, see Fig. 3.

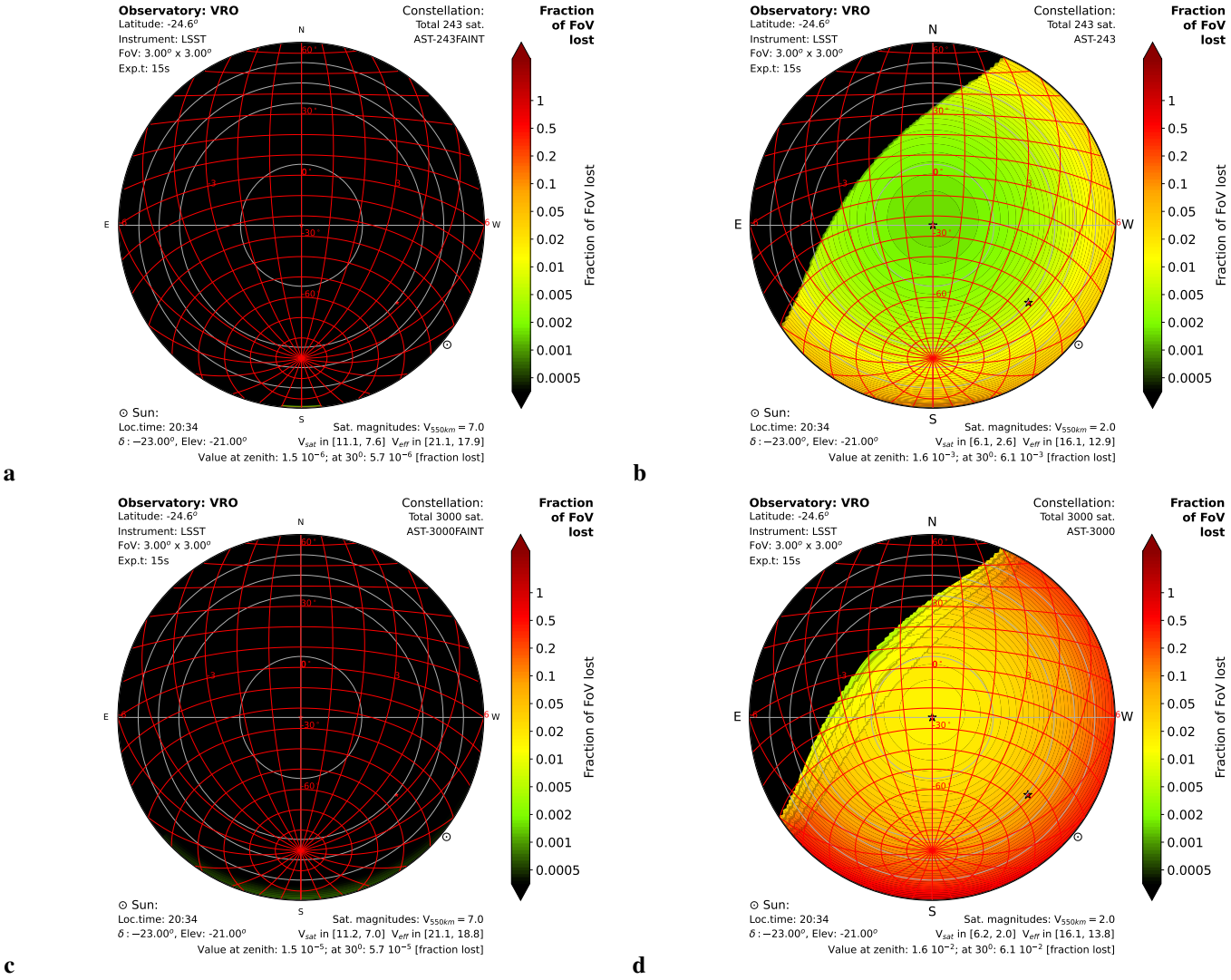

Fig. A.4. FoV losses for a saturating camera, such as LSST, for constellations of 243 satellites (a, b, code AST in the table) and 3000 satellites (c, d, code D3000 in the table) representing BlueBird-like spacecrafts. In panels a and c, the satellites respect the $V < 7$ limit; in panels b and d, they have the measured BlueBird brightness, $V = 2$, i.e. 100× brighter than the limit. For more details on these sky maps, see Fig. 3.

Appendix B: Sky brightness unit conversion

This appendix summarizes the brightness quantities, units, and conversions used in this paper. The conversions are presented as nomograms in Fig. B.1 and B.2.

B.1. Radiometric and photometric brightnesses

Brightness can be expressed as power (in SI units, Watt), possibly per unit surface, per unit solid angle, and over the full spectrum or a restricted band. Such quantities are 'radiometric'.

When the same quantities are weighted by the response curve of the human eye in photopic vision, as defined by the International Commission on Illumination (CIE), they describe perceived brightness. The SI units for these quantities are called (confusingly for an astronomer) 'photometric'. In what follows, we will systematically specify whether "photometric" refers to the perception measurement or the branch of astronomy measuring the brightness of celestial objects.

Astronomical bandpasses are defined by standard photometric systems, such as Johnson–Kron–Cousins *U, B, V, R, I* and Sloan *u', g', r', i', z'*. The Johnson–Kron–Cousins *V* band is, by construction, a good match to the photopic eye response: it peaks near $\lambda \sim 555$ nm and extends roughly from 400 to 700 nm.

Radiometric measurements in *V* can therefore be converted into perceptual photometric quantities. Vision peaks at a shorter wavelength (~ 500 nm), but for this paper we neglect the differences between the various definitions of the *V* filter and the exact CIE response curve.

B.2. Illuminance, irradiance, and magnitude

The total flux of a celestial source through a *V* filter, incident on a surface per unit area, is the 'irradiance', measured in W m^{-2} . It is obtained by integrating the spectral flux density $f(\lambda)$ (in W m^{-2} μm $^{-1}$) over the filter response curve $V(\lambda)$:

$$F_V = \int_0^\infty f(\lambda)\, V(\lambda) d\lambda. \tag{B.1}$$

Alternatively, the flux density can be expressed per unit frequency; a customary non-SI unit is the Jansky, with 1 Jy = 10^{-26} W m^{-2} Hz^{-1}.

The 'magnitude' of an object is the logarithmic counterpart of irradiance. It is defined as

$$m_V = -2.5 \times \log_{10}\left(\frac{\int_0^\infty V(\lambda)\, f(\lambda)}{\int_0^\infty V(\lambda)\, f_o(\lambda)}\right), \tag{B.2}$$

where f_0 is a reference flux corresponding to $m = 0$. The factor $-2.5\log_{10}$ preserves the historical magnitude scale going back to Hipparchus (120BC). We work in the Vega system, in which Vega has $m = 0$ in every filter (Johnson & Morgan 1953). Other systems exist, for example the AB system, where f_0 is constant and equal to 3631 Jy. In the *V* band the AB–Vega offset is only $\sim$ 0.02 mag (Blanton & Roweis 2007), negligible for our purpose.

Formally, Eqs. B.1 and B.2 require the response curve $V(\lambda)$ and the source spectrum $f(\lambda)$. As we work with reflected solar light, we use $V_\odot = -26.75$ (Cox 2000) and integrate the 2008 Whole Heliosphere Interval (WHI) Solar Irradiance Reference Spectra[16] (Woods et al. 2009) over a generic Bessel *V* transmission curve. This gives $F_{V,\odot} = 164$ W m^{-2} and therefore

$$F_V = 164 \times 10^{-0.4(m_V+26.75)}. \tag{B.3}$$

[16] https://lasp.colorado.edu/lisird/data/whi_ref_spectra

The perceptual photometric counterpart of irradiance is the 'illuminance', whose SI unit is the lux (lx), equivalent to lumen per square metre (lm m^{-2}). For monochromatic light at $\lambda = 555$ nm, where the eye is most sensitive, 1 lx = 1.464×10^{-3} W m^{-2}by SI definition. A traditional non-SI unit is the foot-candle (fc), defined as the illuminance on the inside of a one-foot sphere produced by a one-candela source at its centre. Hence

$$1\ \mathrm{f}c \simeq 10.764\ \mathrm{l}x. \tag{B.4}$$

Krisciunas & Schaefer (1991) relate the magnitude of the Moon m_V to its illuminance *I*, expressed in foot-candles, as

$$I = 10^{-0.4(m_V+16.57)}. \tag{B.5}$$

B.3. Luminance and surface brightness

For an extended source — for example a nearby galaxy or the sky background — brightness per unit solid angle is often more useful than total brightness.

The irradiance per unit solid angle is the 'radiance', in W m^{-2} sr^{-1}. Astronomers, however, often use square arcseconds, with the conversion

$$(1'')^2 = \frac{\pi}{180 \times 3600}[sr], \tag{B.6}$$

and therefore often express radiance in W m^{-2} arcsec^{-2}, and spectral radiance in W m^{-2} arcsec^{-2} μm $^{-1}$.

The logarithmic equivalent for extended sources is the 'surface brightness', expressed in magnitudes per square arcsecond (MpSA). Its definition is the same as Eq. B.2, replacing the spectral flux density by the spectral radiance $I(\lambda)$:

$$M_V = -2.5 \times \log_{10}\left(\frac{\int_0^\infty V(\lambda)\, I(\lambda)}{\int_0^\infty V(\lambda)\, f_o(\lambda)}\right). \tag{B.7}$$

Using the same *V*-magnitude to flux relation as for irradiance (Eq. B.3), together with the square-arcsecond to steradian conversion (Eq. B.6), the relation between surface brightness M_V and the radiance through the *V* filter I_V, in W m^{-2} sr^{-1}, is

$$I_V = \left(\frac{180.0 \times 3600.0}{\pi}\right)^2 \times 164.346 \times 10^{-0.4(M_V+26.75)} \tag{B.8}$$

$$= 6.992 \times 10^{12} \times 10^{-0.4*(M_V+26.75)}. \tag{B.9}$$

$$\tag{B.10}$$

Another commonly used non-SI unit is S_{10}, defined as the surface brightness corresponding to a 10th-magnitude star spread over one square degree. The conversion is

$$1\ \mathrm{S}_{10} = 27.78\mathrm{MpSA}. \tag{B.11}$$

The perceptual photometric counterpart is the 'luminance', expressed in candela per square metre (cd m^{-2}), which we use here. A common non-SI unit is the Lambert (L), defined as

$$1\ \mathrm{L} = \frac{10^4}{\pi}\ \mathrm{cd\ m^{-2}} \simeq 3183.1\ \mathrm{cd\ m^{-2}}. \tag{B.12}$$

The conversion between radiometric and perceptual photometric units again depends on the source spectrum. For reflected sunlight, we use the calculations of Bará (2019) for a $T = 5500$ K blackbody in the *V* filter (their Table 1 and Eq. 10):

$$L_V = 10.987 \times 10^4 \times 10^{-0.4 M_V}, \tag{B.13}$$

with M_V in MpSA and L_V in cd m^{-2}.

Finally, Bortle (2001) introduced a nine-class scale of sky darkness, from Class 1 for the darkest skies to Class 9 for inner-city skies. These classes have since been quantified in MpSA.

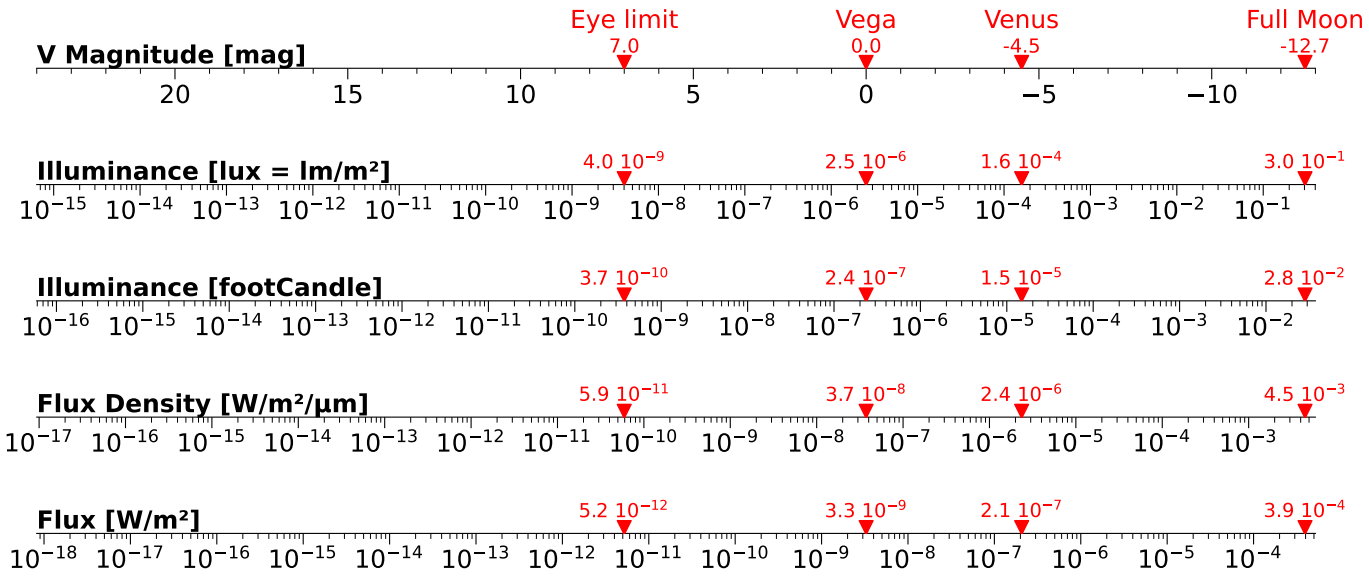

Fig. B.1. Conversion between magnitude, irradiance, and illuminance in the *V* filter for solar spectra.

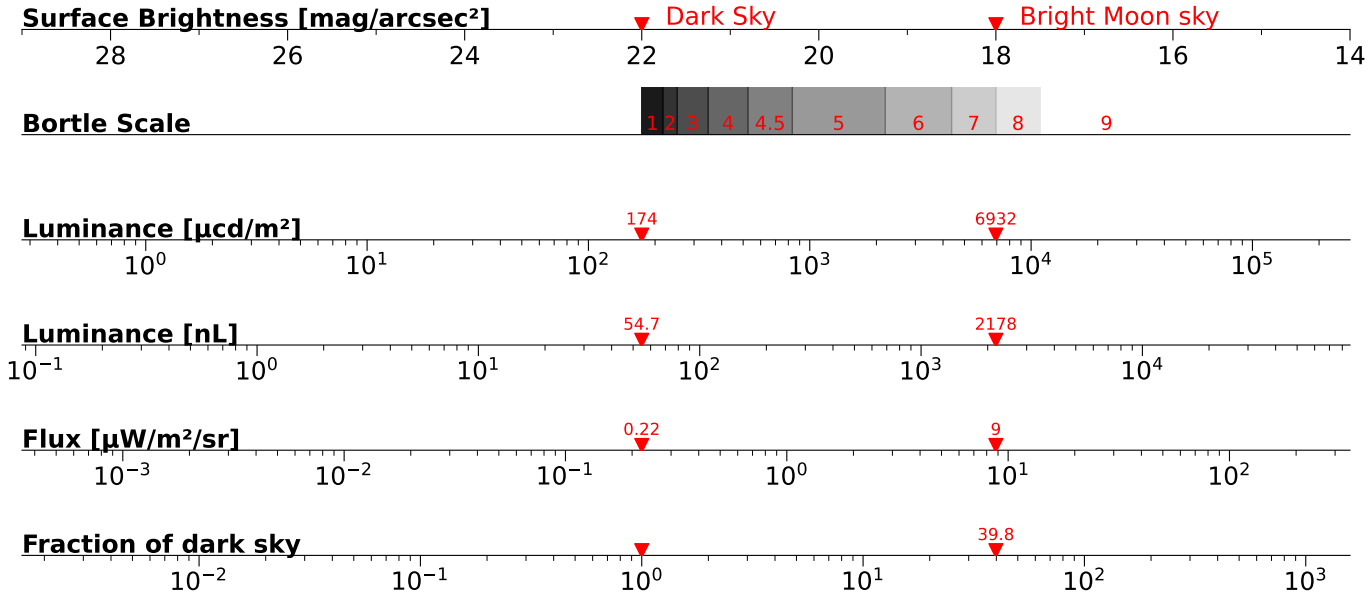

Fig. B.2. Conversion between surface brightness, radiance, and luminance in the *V* filter for solar spectra.